FRACTURE AND FLOW IN

NORMAL AND ANOMALOUS GLASSES

by

M.R.BACHE, BA

A thesis submitted to the University of Keele for the Degree of Doctor of Philosophy

Department of Physics
University of Keele
Keele, Staffordshire

now at

Department of Materials Engineering
University College of Swansea
Swansea, West Glamorgan

October 1988

ABSTRACT

Spontaneous crack extension in fused silica glass when immersed in alkaline solutions but in the absence of an applied stress will be described. In addition, indentation tests on soda-lime-silica and fused silica employing pyramidal indenters with three different included angles will be discussed.

ACKNOWLEDGEMENTS

I would like to express my appreciation to my supervisor Dr. D.G. Holloway for his stimulus and persistant encouragement during the programme of study that eventually resulted in this thesis.

I would also like to thank the following:

Professor W. Fuller	for the provision of laboratory facilities
Mr.F.Rowerth / Mr.W.Robinson and Messrs.G.Dudley, G.Marsh and E.Greasley	for excellent technical and workshop support
Mr.M.Cheney	for electron microscopy
Mr.M.Daniels	for the preparation of the thesis photographs
Dr.G.Lees and Mr.D.Emery	of the Geology Dept., Univ. of Keele, for the X-Ray fluorescence analysis
University of Keele	for financial support
and my wife, Kay	for originally encouraging me into post-graduate study and her help to see it through

Finally, to the remaining technical staff in the Physics Department at Keele too numerous to mention, I include the following quotation in gratitude of their friendship:

"There are three roads to ruin; women, gambling and technicians. The most pleasant is with women, the quickest is with gambling, but the surest is with technicians".

Georges Pompidou (1911-1974)

SYNOPSIS

Although it is now generally agreed that glass exhibits some form of permanent deformation under an indenter, the role of plastic flow in the fracture process is still controversial. In the early stages of the work described in this thesis, some preliminary experiments were carried out on two different phenomena which, it was felt, might add useful information about the flow and the fracture processes. The initial results seemed interesting and it was realised that the intermittent nature of the experimental routines made it simple and efficient to continue with both investigations running in parallel, rather selecting one of them for detailed exploration.

In this thesis it will be convenient to describe the two investigations separately and to discuss the individual results before, finally, considering their possible contribution to our understanding of the fracture process in glass.

The first part of the thesis will be concerned with the study of spontaneous cracking in fused silica glass when it is immersed in particular alkaline solutions but in the absence of any applied stress. An account of the experimental methods used to explore the process and the results obtained is followed by a discussion of the nature of the phenomenon. It is suggested that the cracking is due to the extension of pre-existing surface microcracks under mechanical stresses developed in the course of a chemical interaction between the silica glass and the alkaline solutions. The form of the reaction is not clear, but some

simple calculations give some idea of the possible numbers of ions involved.

In the second part, an investigation of the phenomena associated with indentation of the surface of silica and soda-lime-silica glass is described. Series of indentation tests, using three indenters with different interfacial angles, were carried out and the features produced beneath the indenter were examined by virtual sectioning of the indent as well as by a novel etching technique. Shear flow lines were found beneath indents on soda glass for all three indenters and it will be argued that this indicates that the criterion for flow can not be simply the tensile surface strain imposed by the indenter; no flow lines were found in silica glass.

Finally, with some disappointment, we shall conclude that although effects of intrinsic interest have been explored, as yet they do not appear to shed much light on the role of plastic flow in the fracture of glass.

CONTENTS

CONTENTS (continued)

CONTENTS (continued)

CHAPTER ONE

INTRODUCTION

Despite its brittle nature, glass has been chosen for a variety of uses over many centuries, often because of its apparent chemical inertness. Research over recent decades, however, has demonstrated that glass should not be considered as an ideally brittle material and that under some conditions chemical reactivity can be seen to play an important role in its mechanical behaviour.

The criterion for fracture of an ideal, perfectly brittle material was presented in the much cited paper by Griffith (1920) which was probably the first attempt at a quantitative approach to the mechanics of fracture. Crack propagation in elastic solids was considered essentially in a thermodynamic manner using the principle of energy conservation: propagation proceeds by the conversion of elastic energy, stored in the body containing the crack and in the loading system, into surface free energy of the fracture surfaces. Detailed analysis shows that this energy-balance criterion for crack propagation in an elastic solid can be expressed as:

$$-\frac{\delta U}{\delta A} \geq \frac{\delta T}{\delta A} \qquad [1]$$

where U is the stored elastic energy, T is the surface free energy and A is the area of the newly formed crack surfaces.

Hence for ideal brittle fracture the elastic energy released would be equal or greater than the free energy of the newly formed surfaces during crack extention. However,

most materials exhibit additional energy dissipating processes near to the crack tip and in such cases the released elastic energy would need to provide both the surface energy and the energy expended in the material, P, at the crack tip. Therefore:

$$T + P = \beta \qquad [2]$$

where β is the fracture surface energy of a real solid. Many studies of the slow crack propagation into virgin glasses have highlighted an additional deviation from ideally brittle behaviour: that of environment sensitivity. A variety of test conditions have been employed including air (at different humidities, temperatures and pressures), water, alchohols and liquid nitrogen. From these tests a general agreement has emerged that water plays a dominant role in the fracture process.

Reports by Kies and Clark (1969), Schonert, Umhauer and Klemm (1969), Wiederhorn (1967) and Weidmann (1973) presented remarkably consistent results for slow crack propagation in dry/vacuum, moist air and liquid environments. The typical curves found by these authors are illustrated in Figure 1.1 . The results consistently show that the curves of log(crack speed) against strain energy release rate , G, are independent of environment at high values of G. But, for values of G, lower than about 8 Jm^{-2}, the curves show an environment dependence governed by humidity. At the lowest values of G, Figure 1.1 shows the curves for water and moist air tending towards a limiting value, suggesting that below some critical value of G, crack propagation may not occur. However, it is not

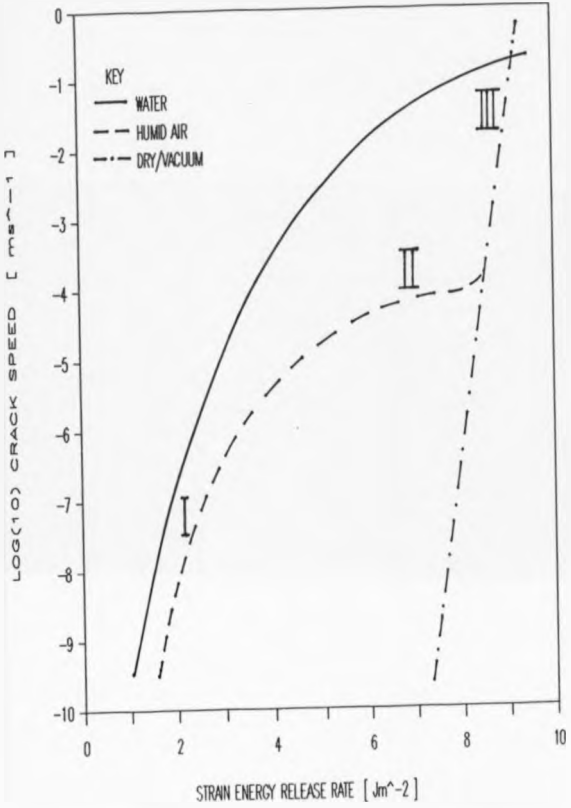

FIGURE 1.1 $Log_{(10)}$ crack speed against Strain Energy Release Rate for crack propagation in glasses under dry-vacuum, humid air and water environments.

obvious what magnitude to assign to this limiting value.

Wiederhorn (1967) considered that the curves of log(crack speed) against G in humid air reflected three distinct stages of crack growth: Region I at low values of G; a second intermediate stage Region II, where the crack speed is virtually independent of G and finally, Region III where the environment-independent cracking occurs at high values of G. This third region was later assigned the descriptive term of *instantaneous fracture* by Weidmann and Holloway (1974b).

The simple energy balance criterion put forward by Griffith (equation [1]), to describe crack propagation also implies, however, that the reverse process, i.e. crack healing may be expected if:

$$-\frac{\delta U}{\delta A} < \frac{\delta T}{\delta A} \qquad [3]$$

Crack reversal is rarely observed; indeed because of the complications introduced by plastic processes during propagation it may be that only ideally brittle materials would be expected to exhibit such a phenomenon. For semi-brittle materials that undergo plastic deformation at the crack tip, crack extension will often cause irregularities on the crack surfaces. Upon the removal of the applied load, although the relaxing elastic field around the crack will attempt to bring the fracture surfaces together, the surface irregularities will prevent complete surface contact and the crack essentially remains open. Although in very brittle materials smooth fracture surfaces may be produced they are often accompanied by surface steps,

striations or debris which can also wedge the crack and prevent closure.

Under controlled conditions glass does exhibit crack healing although this may not have been realised until the 1960's when numerous workers were applying fracture mechanics and slow crack propagation tests to glass. Finkel and Kutnik (1962a+b) reported that cracks in soda glass plates propagated and closed upon the application and removal of bending moments. Outwater and Gerry (1967) described cracks which became invisible upon unloading and remained so until reloaded. The load bearing characteristics of healed cracks in soda-lime-silica glass were quantified by Wiederhorn and Townsend (1970) while Stavrinidis (1980) extended such work to encompass healing in fused silica glass and some of the effects of environment on the healing phenomenon. Stavrinidis found that healed cracks were not only load bearing, i.e. a finite load was required for repropagation, but with aging or annealing the strain energy required for repropagation, G_r ,approached that necessary for very low speed propagation in virgin glass, G_v, (Figure 1.2).

Although the healing of cracks has been established in a range of glasses, it is clear from the effects of time and environment that the process responsible does not represent true crack reversibility as predicted by the Griffith energy balance criterion. The energy for repropagation, G_r , was commonly found to be significantly greater than the normal surface free energy of those glasses.

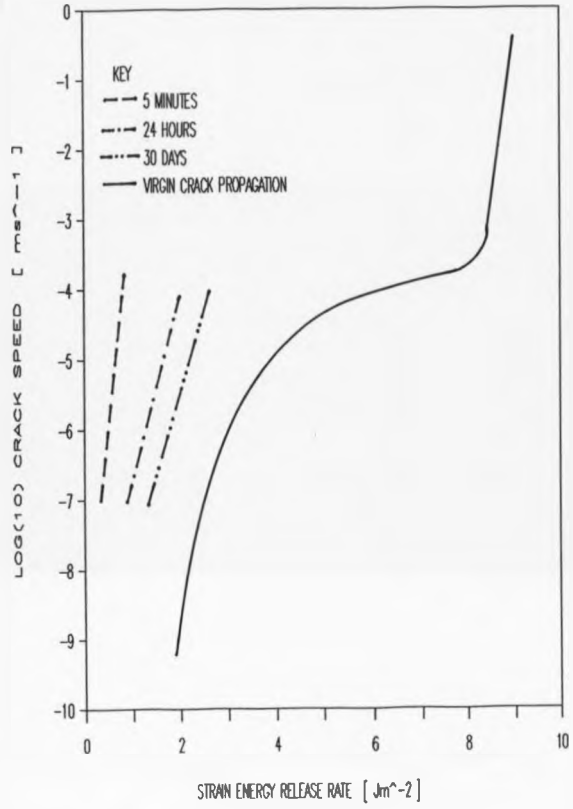

FIGURE 1.2 $\text{Log}_{(10)}$ Crack speed against Strain Energy Release Rate for the repropagation of aged, healed cracks compared to the propagation of virgin cracks in air (soda-lime-silica glass, after Stavrinidis + Holloway 1983).

Stavrinidis and Holloway (1983) concluded that water, in particular, played an important role in the crack healing process. During the initial propagation of the crack, water from the atmosphere will adsorb onto the newly formed fracture surfaces. As the applied stress is relaxed and G is reduced below a critical, but still finite, level crack closure occurs. This brings the once open fracture surfaces together again and an initial adhesion may be possible due to hydrogen bonding between the opposing layers of water molecules adsorbed from the atmosphere. The evidence supporting an increase in adhesion with time or annealing, i.e. the increase in G_r required for repropagation, suggests that the early hydrogen bonding process is then followed by a progressive interaction between the surface layers, now incorporating water, and the SiO_2 network of the bulk glass. Michalske and Fuller (1985) supported the role of hydrogen bonding in the glass healing process and provided a theoretical model of hydrogen bonded linkages which successfully predicts the energy required to repropagate or reopen cracks.

By contrast, tests carried out by Weidmann (1973) using dry liquids such as paraffin and dimethyl sulphoxide (DMSO) demonstrated that, at low values of G, trace amounts of water suffice to increase the rate of crack propagation. Hence, water can either promote crack healing or crack propagation depending upon the energy available to the crack.

Explanations of environmentally enhanced crack propagation are usually made on the assumption (not always

made explicit) that the material is ideally brittle; i.e. any inelastic deformation zone at the crack tip is considered negligibly small, Michalske and Frieman (1983), Lawn (1983) and Frieman (1985). However, an alternative school of thought, which supports a process of limited plasticity at the crack tip even in glass, has been proposed as a possible solution to the longstanding, fundamental anomally in the energetics of glass fracture: the normal fracture energy exceeds the surface energy by a substantial factor. A zone is envisaged ahead of the advancing crack tip within which some form of inelastic or other energy dissipating process occurs prior to rupture. To date, no model has been proposed to explain the transition from flow to rupture in the zone around a crack tip. However, if such a zone did precede an advancing crack tip, water might assist propagation either by reducing the local stress necessary to form the zone or by causing an earlier transition from flow to rupture.

An understanding of the long term durability of glass, the attack on normal glass surfaces under zero applied load by water or aqueous solutions, is also incomplete. Perhaps the earliest recognition of surface corrosion in water was made by Lavoisier (1770). Upon distilling water in a glass vessel, a white precipitate formed, equal in weight to that lost by the vessel, whilst the weight of water remained unchanged. Subsequent technological advances offer detailed chemical analyses of leached glass surfaces, but, often, durability is still measured simply by grading different glasses relative to each other according to their

appearance after exposure to similar test environments.

Chemical analysis has shown that for glass in contact with aqueous solutions alkali ions are extracted into solution to leave an alkali deficient / silica rich surface layer; Pantano, Dove and Onoda (1976), Hench and Clark (1978). The formation of this layer makes further alkali extraction increasingly difficult as the alkali ions have to diffuse from ever deeper in the bulk glass; it has, for instance, been observed that the rate of extraction of alkali ions from commercial silicate glasses falls with the square root of time, Douglas and Isard (1949). Hydrogen ions supplied by water in the solution were suggested as the replacement for the leached alkali by Charles (1958). More recently Paul (1977) and Ernsberger (1980) have both proposed that although charge neutrality is maintained by such an exchange the field intensity of a bare proton would not allow it to exist in a condensed phase. Rather, they suggest, the proton is probably accompanied by water to form a hydronium ion, H_3O^+.

No attempt will be made here to enter into the complexities of leaching at glass surfaces. However, from the basic ideas of the ion exchange process the possibility of a physical or structural change at the glass surface can be envisaged. Differences in the radii of the ions involved in any exchange at the glass surface could cause surface shrinkage or swelling and this might have a direct influence on crack propagation. For example, claims that surface shrinkage can lead to crazing and exfoliation have been made by Metcalfe, Gulden and Schmitz (1971), while the

technique of ion stuffing to force glass surfaces into compression so as to increase the resistance to crack initiation or propagation, is common in the production of toughened glass, Nordberg, Mochel, Garfinkel and Olcott (1964), Fine and Danielson (1988).

The role of surface flaws in limiting glass strength was realised by Griffith (1920). The slow crack extension from microscopic surface cracks is now widely accepted as the cause of fatigue in abrasion damaged glass. The initial, slow extension is followed by rapid crack growth and failure of the specimen. Examples of crack extension have been reported, however, in specimens under zero applied load. Despite the lack of an externally applied load, a finite stress must be present at the crack tip to produce propagation, i.e. a value of $G \geq G_v$ is required. Hence, this must be provided by the corrosion mechanism.

Newton, Holloway and Hench (1979) have reported examples of cracks that could have extended by some form of spontaneous cracking process under zero applied load in specimens of weathered Roman and medieval stained glasses. Features were regularly found which superficially resembled corrosion pits, but in fact showed conchoidal markings and striations on their surface and are semi-ellipsoidal in form. To create these oyster-shell or lenticular shaped fractures a surface crack must have extended into the bulk but for some reason then turned back towards the surface. Similar fractures have been recognised in a partially developed state, where the fragment of glass has not spalled away from the surface and the crack tip is still

within the bulk material. Adams (1974) was able to produce such features in modern glasses by a process of annealing, abrasion, and subsequent soaking in water. Newton et al also described a lenticular fracture on the inside surface of a modern borosilicate glass reflux condenser which had suffered mechanical damage by impact. It should be pointed out that although the mechanical damage was the probable cause of the initial flaw the lenticular crack propagation was believed to have been produced by the environmental attack which followed. This particular example suggests that the presence of a temperature gradient in the glass may contribute to forcing the crack to turn back towards the surface rather than continuing into the bulk. An illustration of the oyster shell / lenticular cracks described by Newton et al (1981) is included in Figure 1.3.

The environmental pH during the leaching process at glass surfaces has drawn regular attention. Continuous leaching by a small quantity of solvent will obviously lead to an alteration in the concentration as ions are exchanged between solution and glass. Although acids (with the notable exception of hydrofluoric acid) show little reaction with glass, strongly alkaline solutions will readily dissolve many silica-based glasses to leave a clear, smooth surface, Doremus (1973).

The effects of alkaline solutions on glass are not so straight forward when metal ions are added to the solution, as they act as inhibitors and reduce the rates of attack, Hudson and Bacon (1958). Calcium was found to act in such a manner by Oka, Ricker and Tomozawa (1979), and in further

Figure 1.3

Oyster shell or lenticular fractures in a borosilicate glass reflux condenser (after Newton et al (1981)).

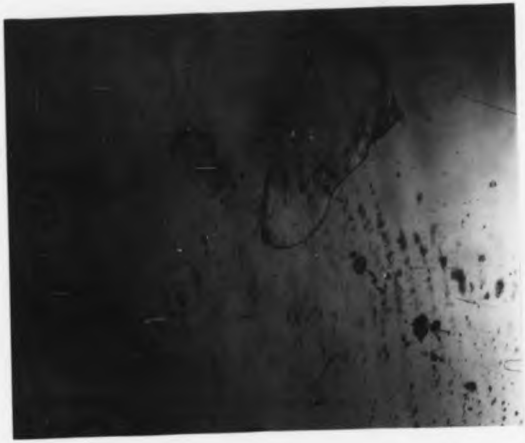

experiments at the same research institute, Tomozawa, Oka and Wahl (1981) discovered an unusual phenomenon which, as will become apparent, largely inspired the experiments reported in this section of the present thesis. The addition of the heavier, alkaline earth ions, barium and strontium, to 1N NaOH caused spontaneous cracking in the surface of fused silica specimens at 80°C. Under identical test conditions, the severity of cracking was greatest on specimens tested in solutions containing barium, which lead Tomozawa et al to suggest that the larger the atomic weight of the alkaline earth element in solution the greater the tendency for surface cracking.

By exposing abraded specimens to these solutions it was discovered that the spontaneous cracking was enhanced by pre-existing surface cracks. Not suprisingly the cracking lead to a dramatic reduction in the mechanical strength of the samples. Fused silica rods were treated for fourteen hours in either 1N NaOH or 1N NaOH + 0.001 gram mol per litre $BaCl_2$ at 80°C followed by mechanical strength tests under four point bending. The mean strength of the rods treated in the barium doped solution fell to about one fifth of those treated in sodium hydroxide.

Since the alkali content of this type of glass is extremely low, Tomozawa et al dismissed the possibility that interaction with the solutions lead to the development of surface stresses by the exchange of ions of dissimilar size. Instead, they proposed a theory of chemical wedging; they suggested that the alkaline earth ions were deposited in pre-existing microcracks and that increasing deposition

would force the crack walls apart and cause the crack to extend. Regardless of the mechanism, however, it was recognised that this phenomenon might be of particular practical interest for the detection of previously sub-microscopic surface cracks.

These observations suggested further experiments would be of interest and an extension of this work formed a major part of the present study of the spontaneous self-extension of cracks under zero applied load. The opportunity was taken to examine the effects of alkaline solutions on soda-lime-silica glass as well as a variety of commercial fused silica glasses of different manufacture and trace element compostion. A variation of the test solutions was initially considered important in an attempt to verify the dominant chemical constituent causing cracking together with the study of the temperature dependence of the process.

Tomozawa et al found more extensive solution cracking on abraded surfaces. However, it is not clear to what extent this effect arises from the repropagation of cracks which have healed during the post-abrasion relaxation rather than by the extension of the surface microcracks into virgin glass. Experiments were therefore designed to attempt to determine the dominant process occuring with the chosen solutions and materials.

CHAPTER TWO

EXPERIMENTAL METHODS

2.1 Introduction

The present chapter describes the apparatus and techniques employed to examine the propagation of both macroscopic and microscopic surface cracks in soda lime silica and several fused silica glasses in various test environments.

The preparation of specimens to acheive different surface conditions and the use of a double torsion machine to produce specimens containing macroscopic cracks are described. Crack extension under both zero and finite applied loads and the repropagation of healed cracks will be discussed.

2.2 Materials

Two different glass compositions were used during testing: soda-lime-silica (soda) and fused silica glass.

The soda glass took the form of 1 mm thick microscope slides (Select microslides, Chance Propper Ltd.) or 3 mm Float glass (Pilkington Bros. Ltd.).

Five different grades of fused silica were used, supplied by either Thermal Syndicate Ltd. or Heraeus Ltd.. The chemical composition of all five grades is quoted as at least 99.9% SiO_2, plus trace quantities of other elements. The five do differ, however, according to their process of manufacture and surface finishing. The form and dimensions of the five grades as supplied together with relevant

comments are included in Table 2.1.

The nominal compositions of the soda and fused silica glasses are presented in Table 2.2.

2.3 Solution Preparation

The following solutions were used as test environments during different stages of the experimental programme:

a) Distilled water.

b) 1N NaOH.

c) 1N NaOH + 0.001 gram mol per litre $BaCl_2$.

d) 1 litre H_2O + 0.001 gram mol $BaCl_2$.

The solutions were prepared and stored at laboratory temperature using plastic receptacles. The solutions were mixed using distilled water and commercial grade laboratory reagents (British Drug Houses Ltd.).

2.4 Materials Preparation

All types of stock material were cut to conveniently sized samples either by using a diamond impregnated wheel or a score and break technique, depending upon the accuracy of specimen dimensions or the condition of the cut surface finish required.

To produce samples that would later be used to study the propagation of macroscopic cracks, microscope slides, or small plates cut to approximately 2.5 cm wide and from 4 to 7 cm long, were used. A crack was initiated at one end of each plate by making a fine score about 1 cm long on one face with a diamond, taking care to ensure the score was central and orthogonal to the sample edge. Then by tapping

GRADE	FORM	DIMENSIONS	COMMENTS	METHOD OF MANUFACTURE *
VITREOSIL (TS)	Sheet	Ave. thickness 2 mm	Transparent variety, contained some inclusions, rolling furrows and some surface scratches and cracks.	Either: a) Electrical fusion of quartz crystals b) Flame fusion of quartz crystals
	Rod	10 mm diameter	Transparent, no inclusions, microscopically flawless surface.	
SPECTROSIL B (TS)	Rod	10 mm diameter	Transparent, no inclusions, some microscopic surfaces flaws	Flame hydrolysis of $Si\,Cl_4$
	Disc	50 mm diameter 10 mm thickness	Transparent, top and bottom surfaces free from microscopic flaws, ground edges	
HERASIL (H) HOMOSIL (H) SUPRASIL (H)	Rod	All 3mm diameter	All transparent, no inclusions or surface flaws	Flame fusion of quartz crystal
				Flame hydrolysis of $Si\,Cl_4$

TABLE 2.1 Grades and form of fused silica as supplied by manufacturers.
(TS = Thermal Syndicate Ltd., H = Heraeus Ltd., * = after Doremus (1979))

%	Microscope Slides [1]	Float Glass [2]	Fused Silica (All Grades)
SiO_2	72.3	72.7	99.9
Na_2O	13.4	12.9	TRACE QUANTITIES
K_2O	0.6	0.6	
CaO	9.0	9.0	
MgO	3.1	3.1	
Al_2O_3	1.0	1.0	
Others	0.7	0.7	

(1) Chance Proper Ltd.
(2) Pilkington Bros. Ltd.

Table 2.2 Nominal composition of glasses.

gently on the reverse side of the score a short crack was produced. If desired this crack could then be extended to a known length prior to testing using a double torsion machine.

For the study of the behaviour of surface microcracks, specimens were tested either in their as-received condition or after different surface treatments. Ground and polished, sawn and fractured surfaces were each examined as well as surfaces damaged by abrasion with 320 grade silicon carbide paper, indentation with diamond pyramid indenters or simple scratching with a diamond.

2.5 The Double Torsion Machine

Specimens containing macroscopic cracks were produced using a double torsion machine. The machine, designed by the author and based on previous models made in this laboratory by Weidmann (1973) and Stavrinidis (1980), was used to produce controlled cracks of a reproducible crack-front profile and also served as a clamp when studying the repropagation of healed cracks.

The machine and the principle of its operation are illustrated schematically in Figure 2.1 . A torque is applied to the specimen via a pair of pins, P1, mounted on an arm that can rotate about an axis exactly central to these and a second pair of fixed pins, P2. The shaft of the rotatable arm is contected to a pulley wheel, A . The rotation of this pulley under an applied force, either by hanging weights from a cord attached to its perimeter or by a displacement of the micrometer loading screw, SL, causes

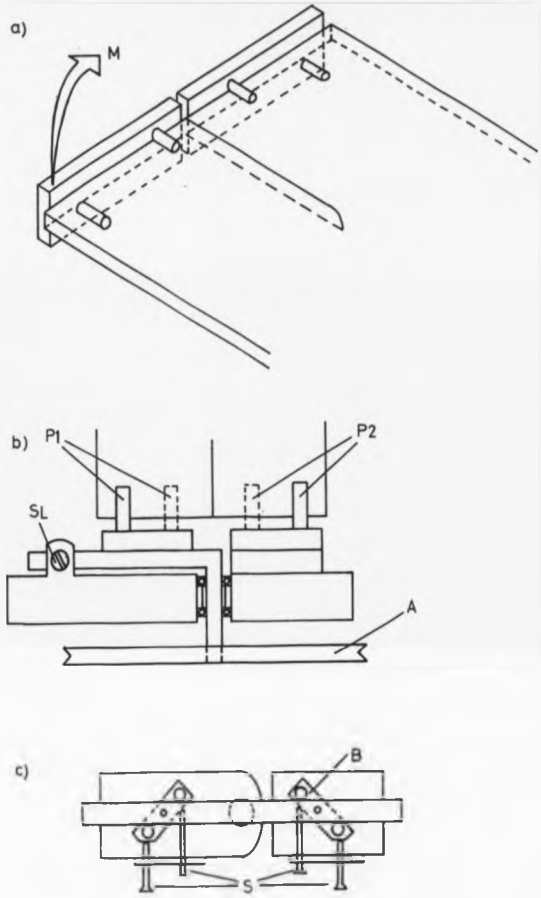

FIGURE 2.1 a) Application of a torque, M, via double torsion b) and c) Lateral and plan views respectively of specimen loading in the double torsion machine.

the rotating pins, P1, to exert a torque on one half of the specimen. This then generates an equal but opposite torque via the fixed pins.

Each pair of pins is hard soldered to separate small steel blocks, B, that can pivot about a central screw so that specimens of different thickness can be accommodated. Once adjusted so that all four pins are in contact with their respective surfaces of a specimen, the blocks can be securely fixed in postion by lateral screws, S. The setting of the pins was important to ensure that straight cracks were produced running centrally in the specimen.

An angled, mild steel framework supports a hinged arm to which the double torsion machine can be attached. The hinged arm facilitates easy insertion of specimens and the double torsion machine can be mounted above or below the arm in order provide the option of propagating cracks vertically upwards or downwards. With the machine below the hinged arm, specimens could also be clamped at their uncracked end and immersed in a test cell to observe healed crack repropagation under zero applied load.

2.6 Production of Macroscopic Cracked Specimens

The double torsion machine was employed to study crack propagation under an applied load or to prepare macroscopic cracks in specimens that would then be immersed in various test solutions under zero applied load.

For crack propagation studies, specimens which had had a crack initiated at one end by the diamond score technique were inserted into the double torsion machine with the

short crack central to the two sets of loading pins. The double torsion machine, attached below the hinged supporting arm, was then lowered so as to immerse the specimen into a cell containing the test solution. A load was applied to the specimen by hanging weights from a cord fixed to the loading pulley (A) and passing over a secondary pulley on the framework.

To produce specimens with macroscopic cracks for use under zero loading, specimens were inserted in the double torsion machine as previously described and the loading arm screw (SL) was employed to propagate a crack at laboratory temperature and humidity to a length approximately three quarters of the total specimen length. With the specimen illuminated at a favourable angle, so that the crack tip was clearly visible, the crack length was measured with a travelling microscope. The maximum extension was marked using a vernier eyepiece and as the load was gradually removed by turning the loading arm screw anti-clockwise any crack closure was measured.

The greatest closure was found with specimens mounted vertically above the machine. This was probably because fracture debris from the diamond scratch or propagated crack could not fall into the crack and wedge it open once the load was removed. With this upwards configuration some cracks closed almost as far back as the original diamond scratch. When it was desired to avoid or limit healing, cracks were propagated vertically downwards.

2.7 Immersion Tests Under Zero Applied Load

For testing at laboratory temperatures, samples with preformed cracks or a selected surface treatment were completely immersed in test solutions held in polythene or perspex trays. The trays were covered to reduce solution evaporation and contamination. Fresh solution was occasionally added if the level fell to the extent that specimens might be uncovered. The test period varied up to maximum of six months.

Specimens for testing at elevated temperature were initially immersed at laboratory temperature in a solution held in a polythene bag within a Pyrex beaker. The bag was tied at the top with wire and the beaker was then transfered to an oven (Hereaus Ltd.) at 80°C. The greatest temperature fluctuations were experienced on opening the oven to remove or replace individual specimens, however, the temperature fall was less than 5°C for ten minutes. Normally the temperature was controlled to within $\pm$ 2°C.

The polythene bag was used to prevent contact between the test solution and the glass (Pyrex) beaker which provided security against any leakage of solution. The duration of the test at 80°C varied but was usually restricted to less than fourteen days by solution evaporation or complete specimen degradation.

Great care was taken whenever removing any specimen from solution for the measurement of crack length or for inspection of the surface. Beakers containing solutions at 80°C were allowed to cool to laboratory temperature before

specimens were removed. Specimens containing macroscopic cracks were transfered to a double torsion machine which served as a clamp while the crack length was measured. Such a specimen was transfered by gripping it with tweezers at its uncracked end, and then the loading arm screw of the double torsion machine was carefully adjusted so that the specimen was just supported in an upright postion. The crack length was measured with a travelling microscope.

Tests at both laboratory and elevated temperature established that the specimen orientation while immersed in solution was of no significance to the rate of crack growth or healed crack repropagation. Normally in prolonged tests, up to six months, the test solution was topped up as needed. But a control test, in which the test solution was carefully replaced with a fresh batch each week over a six month period, demonstrated that the age of the solution during a long term test at laboratory temperature was also of no apparent importance to crack propagation behaviour.

The immediate response of healed cracks to immersion in the test solutions was also studied. Healed, cracked specimens were clamped at the uncracked end so that they hung into an empty test cell below. The crack tip position was noted using a travelling microscope and then the test solution was introduced into the cell. Once the crack was completely immersed and the solution level was above the

crack tip any repropagation was measured as a function of time.

2.8 Specimen Preparation For X-Ray Fluorescent Analysis

A number of fused silica specimens, after testing in selected solutions under zero applied stress, were selected and prepared for X-ray fluorescent spectroscopy.

Following the test immersion, the specimens were carefully removed from the solution, washed under running distilled water for two minutes and then placed in an ultrasonic cleaning bath containing distilled water and a surface decontaminant (Decon 90) for 30 minutes. The specimens were then dried using warm air. The aim of this procedure was to eliminate, as far as possible, any precipitation from the test solution onto the specimen surface and within cracks. A specimen of fused silica in its as-received condition was also subjected to this cleaning procedure.

Fused silica specimens in the following conditions were scanned for barium and sodium content:

a) As received.

b) After 4 days immersion in 1N NaOH + 0.001 gram mol per litre $BaCl_2$ at 80°C.

c) After 6 days immersion in 1N NaOH at 80°C.

d) After 11 days immersion in 1N NaOH at 80°C.

CHAPTER THREE

RESULTS AND PRELIMINARY DISCUSSION

3.1 Introduction

In this chapter the effects of different alkaline soluions on soda-lime-silica and fused silica glasses are presented, with particular attention paid to crack propagation on both the microscopic and macroscopic scale under zero applied load.

The general degradation of the surface of specimens in the different environments will be described qualitatively and illustrated by a series of photomicrographs. The form of microcracking will be discussed in detail.

The behaviour of soda lime silica and fused silica glasses will be described separately with the effects of water, 1N NaOH and 1N NaOH + 0.001 gram mol per litre $BaCl_2$ given prominence. The differences between results obtained at laboratory temperature and 80°C will be highlighted.

Results from tests which were designed in an attempt to discover the mechanisms involved in the spontaneous extension of cracks are then described. These include some quantitative results for the repropagation of healed cracks under zero applied load, the extension of cracks into virgin glass under zero load (the term virgin is used in context of propagating cracks into material that has previously remained unfractured) and the effect of selected solutions on the slow crack propagation under applied load.

To aid comparison of the results of the present study

and those of previous investigations, graphs representing crack propagation rates under applied loads employ the fracture mechanics parameter G, the strain energy release rate.

3.2 Surface Degradation of Soda Lime Silica Glass

Immersion in distilled water produced no obvious visible changes in the surface of soda-lime-silica specimens even after six months at 80° C.

At laboratory temperatures, between 18 and 20°C, none of the selected alkaline solutions had any obvious effect but at 80°C both sodium hydroxide and sodium hydroxide containing barium chloride gave rise to pits on damaged surfaces. Such pits are illustrated in Figure 3.1a; they are steep sided, smooth hollows, often elongated in the direction of scratches around which they have formed and may coalesce to give a "rope coil" appearance. Similar pits occur in the mist zone of a fracture surface as is illustrated by Figure 3.1b . Pitting did not occur on surfaces, such as the mirror zone of fractures, which were free of microscopic abrasions and cracks.

Overall, the effect of alkaline solutions on soda-lime-silica glass appears to be confined to the development of pits at the site of surface microcracks and this contrasts sharply with the behaviour of silica glass to be described below.

Figure 3.1a

Soda-lime-silica specimen, abraded with 320 grade silicon carbide. 8 days in 1N NaOH + 0.001 gmol per litre BaCl at 80°C. Illustrating surface pitting and "rope coil" effect along surface scratches.

Scale: 1mm=7um

Figure 3.1b

Mist zone of a fracture surface on soda-lime-silica after 8 days immersion in 1N NaOH + 0.001 gmol per litre BaCl at 80° C. Illustrating pitting over the mist zone but note the clear area to the bottom of the figure representing a smooth surface on a large mist element.

Scale: 1mm=7um

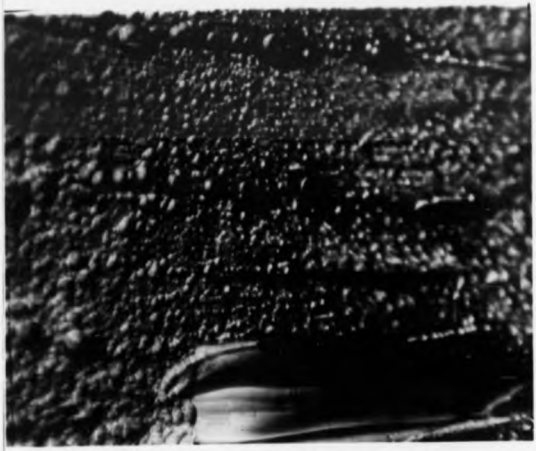

3.3 Surface Degradation of Fused Silica Glass

No fused silica specimen showed any obvious change when immersed in water or alkaline solutions at laboratory temperatures. At 80°C, however, all the fused silicas developed surface microcracks in alkaline solutions. Although the interval before microcracks appeared varied with the solution, and to a lesser degree the grade of fused silica, the general form of microcracking was the same in all cases. The original surface condition of specimens proved critical in the sense that cracking developed from abrasion scratches, indentations, pre-existing macroscopic cracks or extentively on ground and polished surfaces.

Microcracks were also formed on some specimen surfaces where no pre-existing flaws had previously been detected. The only type of surface that failed to develop microcracks was a smooth fracture surface. This is illustrated by Figure 3.2 where cracks can be seen extending into the bulk of the specimen from each surface except the fracture surface facing the viewer.

3.4 Vitreosil in 1N NaOH + 0.001 gram mol per litre $BaCl_2$ at 80°C

The series of photomicrographs, Figure 3.3 to 3.11, illustrate the development of cracks, mostly in Vitreosil, in sodium hydroxide and in sodium hydroxide containing barium chloride. However, similar effects were observed with all the grades of silica examined.

All Vitreosil specimens exhibited surface cracking

Figure 3.2

Spectrosil B after 8 days in 1N NaOH + 0.001 gmol per litre $BaCl_2$ at 80°C. Microcracking on all surfaces except the smooth fracture surface facing the viewer.

Scale: 1cm=3.5mm

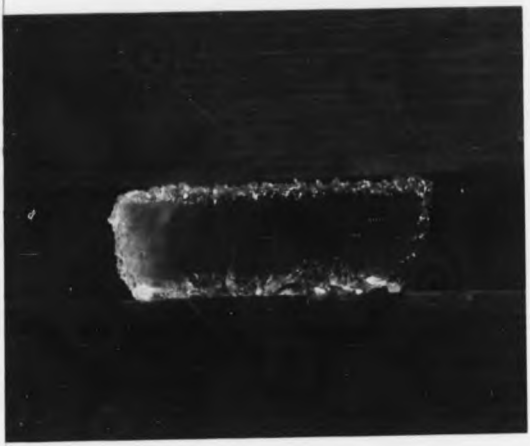

after twenty four hours immersion in 1N NaOH + 0.001 gram mol per litre BaCl, at 80°C although the exact time at which cracks were first detected varied according to the original surface condition. For this reason no attempt was made to measure this "time to earliest cracking". The earliest cracks to appear were commonly isolated and found near to or straddling prominent surface flaws such as scratches, indentations or pre-existing cracks which had some secondary microscopic cracks associated with them. Single lenticular cracks were noted at this stage but after longer immersion times, cracks tended to branch to form complex patterns both on and below the surface, Figure 3.3. The shadow to the bottom of the figure is due to a large number of cracks of random orientation in this region which are reflecting the incident light out of the objective plane. Towards the extremities of this shadow, however, individual crack tips can he seen extending into the bulk and outcropping on the surface. Portions of the specimen surface often spalled away as the increasing number of cracks of random orientation began to intercept or individual cracks turned back towards the surface rather than extending deeper. The specimen surfaces became increasingly friable after a few days, Figure 3.4 .

Figure 3.5, typical of many spalled surfaces at high magnification, illustrates a rod of vitreosil after 8 days. To the right hand side of the photograph is a noticeable pattern of intersecting boundaries apparently marking the intersection between individual, adjacent fractures. The fracture surfaces are marked by a series of lines and these

Figure 3.3

Vitreosil, 8 days immersion in 1N NaOH + 0.001 gmol per litre $BaCl_2$ at 80°C, showing the complexity of cracking.

Scale: 1mm=20μm

Figure 3.4

Vitreosil, 5 days immersion in 1N NaOH + 0.001 gmol per litre $BaCl_2$ at 80°C, illustrating the surface condition of silica specimens after a few days.

Scale: 1cm=5mm

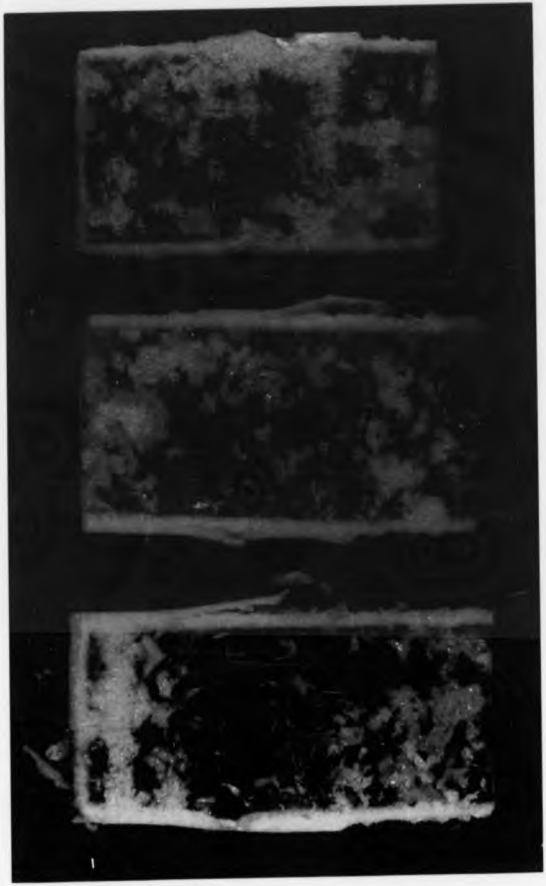

Figure 3.5

Vitreosil, 8 days immersion in 1N NaOH + 0.001 gmol per litre $BaCl_2$ at 80°, illustrating the spalled surface structure of striations and fracture boundaries.

Scale: 1mm=12μm

correspond to steps in the surface.

Figure 3.6 also illustrates such striations and confirms their jagged nature, in this case for a crack which still lies beneath the free surface. The striations extend to an irregular bowed crack front. Two adjacent striations commonly combine into one but at no occasion did any striation branch or split into two.

Optical microscopy at high magnification revealed very feint ripples orthogonal to the striations, although these proved difficult to photograph; some examples are just visible in Figure 3.7.

The influence of surface condition on subsequent cracking is illustrated in Figure 3.8. These two specimens taken from a single length of 10 mm diameter rod, were treated simultaneously in the same solution for 8 days. The left hand specimen was in the as-received condition while the other was abraded with 320 grade silicon carbide prior to testing. Both specimens exhibit wide-spread surface spalling, but the as-received specimen still shows some isolated areas where cracking had not occurred.

Although relatively rare, surface pitting was found on some specimens which had crack free areas after approximately one week.

After 8 days immersion at 80°C in the barium doped solution, most silica specimens had either already disintegrated, or they fell into small pieces on handling.

Figure 3.6

Vitreosil, 8 days immersion in 1N NaOH + 0.001 gmol per litre $BaCl_2$ at 80°C. The jagged striations and irregular bowed crack front are illustrated for a subsurface microcrack.

Scale: 1mm=12μm

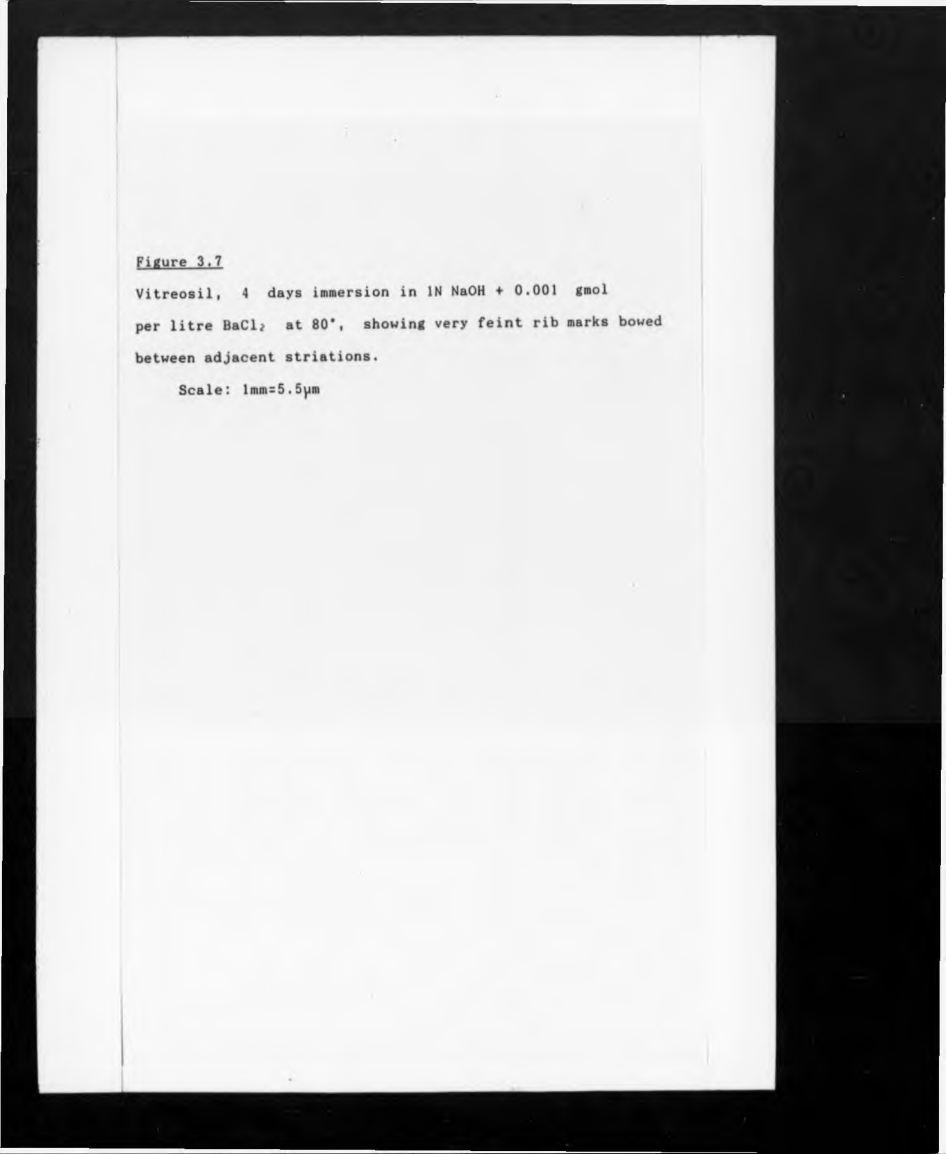

Figure 3.7

Vitreosil, 4 days immersion in 1N NaOH + 0.001 gmol per litre $BaCl_2$ at 80°, showing very feint rib marks bowed between adjacent striations.

Scale: 1mm=5.5μm

Figure 3.8

Vitreosil, 8 days immersion in 1N NaOH + 0.001 gmol per litre $BaCl_2$ at 80°. The specimen at the top was tested in the as received condition, the one at the bottom abraded with 320 grade silicon carbide prior to immersion.

Scale: 1cm≡3mm

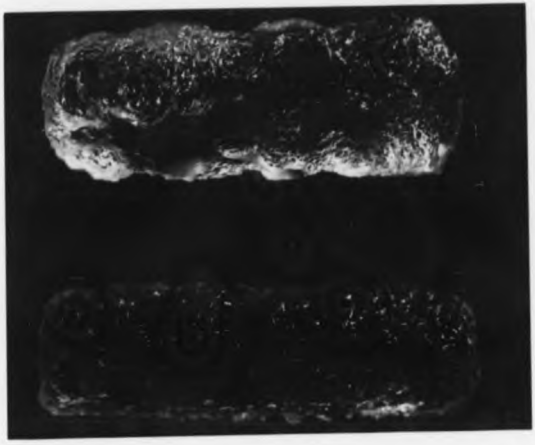

3.5 Vitreosil in 1N NaOH at 80°C

With Vitreosil in 1N NaOH at 80°C the first cracks were not detected until samples had been immersed for about 48 hours, significantly longer than for specimens in the barium doped solution. The subsequent development of cracks also proceded more slowly, although eventually the forms of the cracks and the appearance of specimen surfaces were indistinguishable from those produced in sodium hydroxide containing heavy alkaline earth ions.

Figure 3.9 shows the state of an as-received silica specimen after 8 days in 1N NaOH, and provides a sharp contrast with Figure 3.8. Although this specimen of Spectrosil, prior to immersion, contained a greater number of visible microscopic flaws than the Vitreosil specimens, the rate of attack in 1N NaOH is noticeably slower.

Lenticular cracks, extending into the bulk material but then turning back towards the surface, developed initially from some isolated surface flaws, but with prolonged immersion these became masked by the developing maze of cracking. The internal crack surfaces and crack fronts developed in 1N NaOH showed the same kinds of features (irregular, bowed, sharp crack fronts and jagged striations) as those which developed, albeit more rapidly, in the barium doped solution. However, markedly different behaviour occurred in 1N NaOH towards the end of the second week of immersion. Specimen surfaces were invariably well covered by cracks by this time yet some of these had now developed rounded tips. The crack openings were also widened by the removal of material from the crack walls.

Figure 3.9

Spectrosil B, 8 days immersion in 1N NaOH at 80°C.

Illustrates the generally slower attack at the surface compared to specimens tested in barium doped solution.

Scale: 1cm=3mm

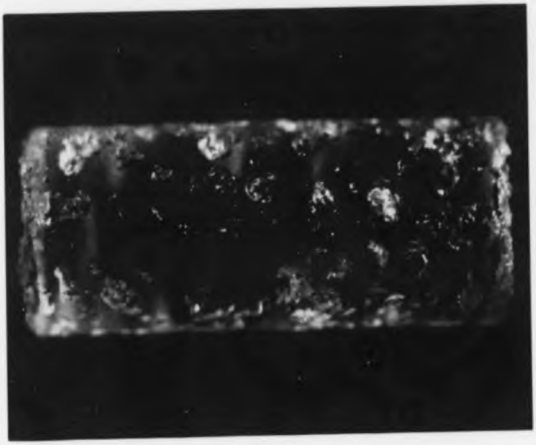

The results of this transition are well illustrated by Figure 3.10, a view of such cracks outcropping on a plane surface. Cracks that had been sufficiently "etched" to allow microscopic examination, possessed smooth crack walls with no obvious fracture markings such as striations or ripples.

Cracks which showed sharp tips and little separation between the crack walls were occasionally found within a few millimetres of those illustrating signs of this etching behaviour. Figure 3.11 shows the track of a surface scratch which served to initiate the sharp cracks now to either side and below the surface, while the scratch itself has etched into a classic, smoothed "rope coil" figure.

3.6 Repropagation of Healed Cracks under Zero Applied Load

Results for the relatively long term repropagation of macroscopic healed cracks under zero applied load, at laboratory temperature and in various test environments are presented in Table 3.1. The figures for average speed of propagation were calculated by measuring, over a period of thirty days, the repropagation of cracks which had closed over a substantial length, at least 5 mm. The results are subject to an error of approximately $\pm 4\%$, arising chiefly from the difficulty in judging the crack tip position to better than 0.1 mm.

Results for the short-term response of healed cracks in soda glass to water and barium doped sodium hydroxide solution at laboratory temperature are presented in Figures

Figure 3.10

Vitreosil, after 14 days in 1N NaOH at 80°C. An open crack with rounded tip outcropping at a plane surface.

Scale: 1mm=12μm

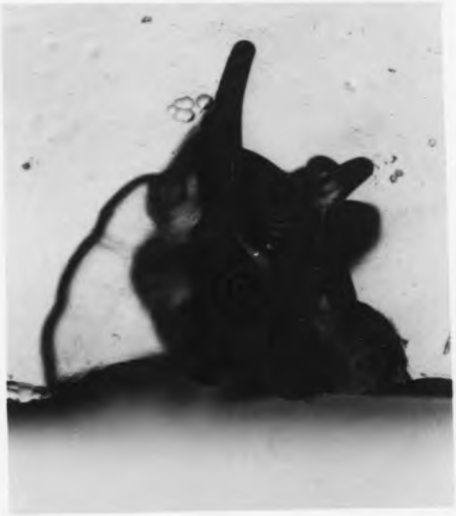

Figure 3.11

Vitreosil, after 7 days in 1N NaOH at 80°C. A surface scratch after etching illustrating a "rope coil" appearance.

Scale: 1mm=12μm

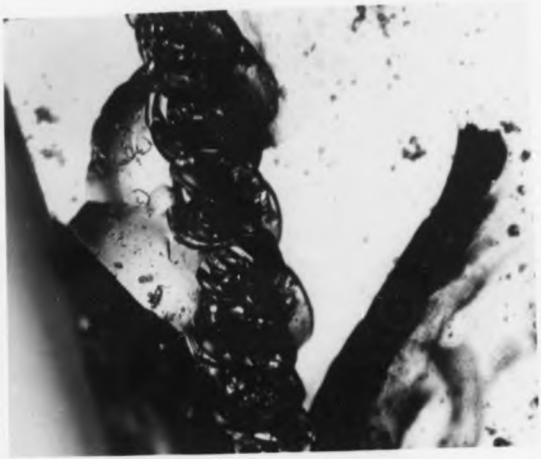

	Soda - Lime - Silica Average Vr (ms^{-1})	Fused Silica Average Vr (ms^{-1})
Distilled Water	4×10^{-9}	1.5×10^{-9}
In NaOH	2.1×10^{-9}	2.2×10^{-9}
In NaOH + 0.001 gmol per litre $BaCl_2$	3.7×10^{-9}	1.4×10^{-9}
1 litre H_2O + 0.001 gmol $BaCl_2$	1×10^{-9}	1×10^{-9}

TABLE 3.1 Average speed of repropagation of healed cracks over 30 days in different solutions.

3.12 and 3.13. Individual specimens were prepared with an initial, open crack of 4 cm long which was then encouraged to heal (the extent of healing is indicated indirectly by the crack length at time t=0). Following the introduction of the test solution, repropagation was measured during the subsequent 30 minute period.

Similar attempts to measure the short term response of healed cracks to solutions at 80°C were unsuccessful. The immersion of specimens at this temperature caused an "instantaneous" repropagation to the original, pre-healed crack length, presumably due to the thermal shock.

3.7 Propagation of Virgin Cracks under Zero Applied Load

At laboratory temperature none of the test solutions caused propagation of pre-formed cracks under zero applied load into virgin glass, in either soda lime silica or fused silica. Whenever the pre-existing crack had healed slightly prior to testing, repropagation occured on immersion in one of the test solutions, but this terminated once the original pre-healed crack length was attained (E.g. the specimen represented by the symbol "X" in Figure 3.12).

At 80°C and under zero applied load, water failed to extend macroscopic cracks in any of the glasses but 1N NaOH + 0.001 gram mol per litre $BaCl_2$ did cause crack extension.

Although pre-existing cracks in fused silica showed extensions at an approximate rate of 10^{-9} ms^{-1} over the first two days immersion, thereafter measuring the crack

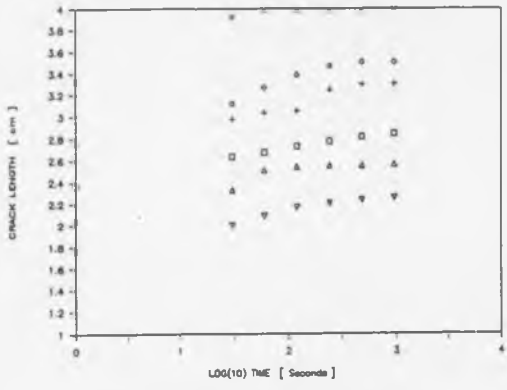

FIGURE 3.12 Short term response of healed cracks in soda-lime-silica to distilled water.

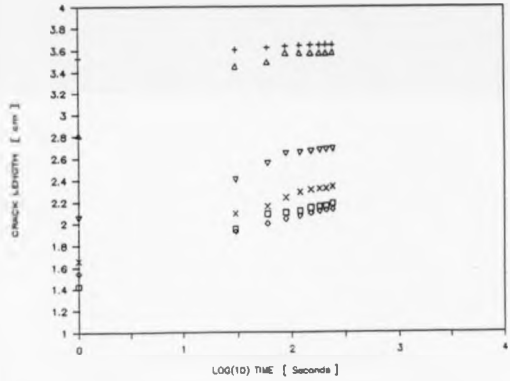

FIGURE 3.13 Short term response of healed cracks in soda-lime-silica to 1N Na OH + 0.001 gram mol Ba Cl_2.

lengths became increasingly difficult because of the development of supplementary surface microcracks: this often obscured the macroscopic crack tip and in addition spalled the specimen edges which had been the reference points for crack length measurments. These problems are well-illustrated in Figure 3.4, where the concentration of surface microcracks almost obliterates the macroscopic crack running central to the length of the specimens and the specimen edges have become extremely irregular. In view of these difficulties any attempt to establish the growth rate for macroscopic cracks in fused silica immersed in sodium hydroxide doped with barium chloride under zero applied load was abandoned.

3.8 Virgin Crack Propagation Under Applied Loads

The results for slow crack propagation under applied loads, as a function of strain energy release rate, in virgin soda-lime-silica glass and various solutions are presented in Figure 3.14 .

For the range of crack speeds from $10^{-7} ms^{-1}$ to $10^{-4} ms^{-1}$, each experimental point represents a mean velocity determined from a crack extension of approximately 5 mm under a constant load. For lower or higher speeds the timed crack extension was varied between 2 mm and 25 mm respectively. No variation in crack speed with crack length was detected on a given specimen under constant load. Each experimental point in Figure 3.14 is subject to an overall uncertainty of about $\pm 20\%$, too small to be represented by error bars on the logarithmic scale. (Details concerning

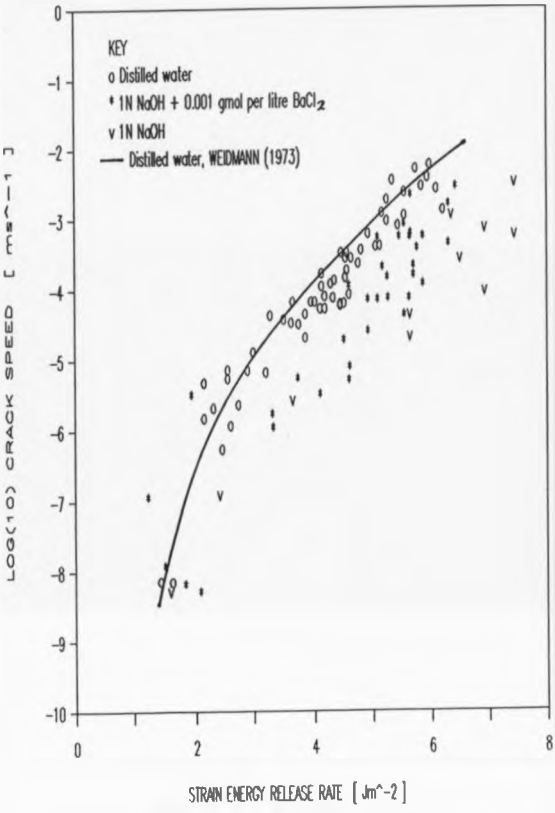

FIGURE 3.14 $\log_{(10)}$ crack speed against Strain Energy Release Rate for soda-lime-silica in various solutions.

the value of this error can be found in an Appendix which describes the use and calibratiion of an angular transducer for the measurement of slow crack speeds).

The results in Figure 3.14 show that within experimental error there is no difference in behaviour between the different solutions, including water.

Since the scatter in the individual results for a given value of G is about one order of magnitude, any effects due to interaction with the solutions must be less than this. It is clear, therefore, that changes in G, (and of course the presence of water) have a much more dramatic effect on the speed of slow crack growth than these alkaline solutions.

Figure 3.15 compares the results for slow crack propagation in fused silica immersed in 1N NaOH + 0.001 gram mol per litre $BaCl_2$ at 20°C, obtained during the present study, with those obtained in water at room temperature by Sakaguchi et al (1982). These measurements of slow crack speeds in fused silica are again uncertain to about $\pm$20% so that for silica glass as for soda-lime-silica, the alkaline solution appears to have no major effect on the speed of crack propagation as a function of strain energy release rate.

3.9 X-Ray Fluorescent Spectroscopy

Figures 3.16 and 3.17 represent the X-ray fluorescent spectroscopic scans for a number of fused silica specimens after various treatments. The plots illustrate activity (kilocounts per second) against angle (degrees). The

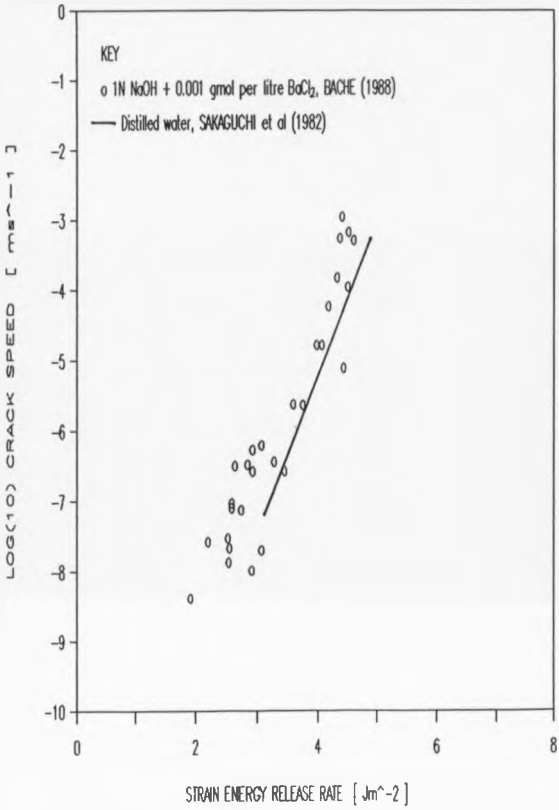

FIGURE 3.15 $Log_{(10)}$ crack speed against Strain Energy Release Rate for fused silica in 1N Na OH + 0.001 gram mol per litre Ba Cl_2.

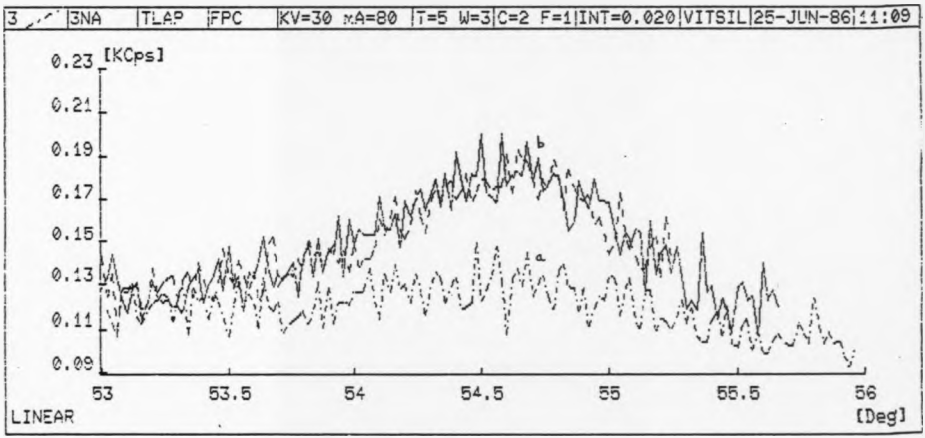

FIGURE 3.16 Plot of Activity against Scanning angle from x-ray fluorescence tests for Vitreosil specimens.
Trace a) = as received material, Na K_α line emission
Trace b) = 2 traces superimposed, of separate specimens after 4 days immersion in 1N Na OH + 0.001 g mol Ba Cl_2, Na K_α lines.

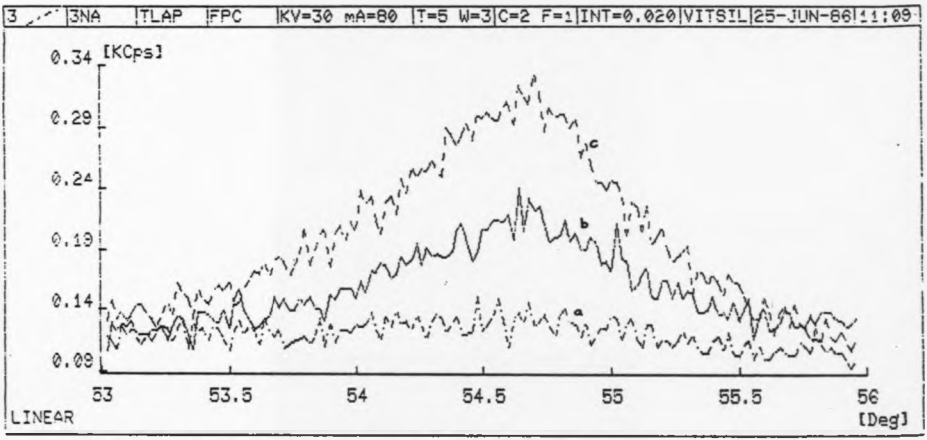

FIGURE 3.17 Plot of Activity against Scanning angle from x-ray fluorescence tests for Vitreosil specimens.
Trace a) = As received material, Na K_{α} line emission.
Trace b) = After 11 days in 1N Na OH at 80°C, Na K_{α} line.
Trace c) = As b) but for a different Vitreosil specimen.

activity from any specimen can be taken as a proportional response from the X-radiation by a chosen element. In this case the scanning range was centred about an angular value of 54.68 degrees in order to detect K_{α} line emissions from the electrons of sodium atoms. Therefore, the two plots are essentially indications of the relative sodium content in each specimen.

Figure 3.16 compares the spectrographs for two separate fused silica specimens that had been immersed in 1N NaOH + 0.001 gram mol per litre $BaCl_2$ at 80°C for 4 days (upper traces) against a specimen of fused silica in its as-received condition. The peak in the spectra of the two treated specimens indicates an increased activity of approximately 70%.

Figure 3.17 illustrates the spectra of two separate silica specimens which were simultaneously immersed in the same solution of 1N NaOH at 80°C for 11 days, compared with that from the as-received material. Increases in activity of approximately 100% and 175% are indicated by the two specimens.

None of the specimens analysed revealed any enhanced activity due to barium.

CHAPTER FOUR

DISCUSSION

4.1 Introduction

Following a brief summary of the results, a phenomenological interpretation of the findings will be suggested and calculations to assess its plausibility will be described. Discussion of the consequences of these present results for the various models for fracture in glass will be reserved until Chapter Eight.

4.2 Summary of Results

Spontaneous cracking was invariably found in fused silica glass but never in soda-lime-silica. For both solutions there was a marked temperature sensitivity; no cracking was seen at laboratory temperatures. The rate of cracking in silica was much more rapid in barium-doped solutions but the process apparently changes to one of dissolution after some time. Dissolution only occurs from the outset in soda-lime-silica. Fused silica alone also exhibited the spontaneous extension of macroscopic cracks.

The spontaneous cracking in silica appears to start from pre-existing surface microcracks. The structure of the fractures is independent of the test solution. Initially, isolated, lenticular-shaped cracks develop with irregular crack fronts and ragged striations. Secondly, tertiary, etc. cracks then develop to form complex families of fractures which leads to the disintegration of the specimen.

Sodium has been detected in the surface layers of silica specimens after immersion. However, despite the enhanced attack in barium-doped solutions, barium itself was not detected.

4.3 Interpretation

The evidence available to date suggests that the spontaneous propagation of microcracks in fused silica is due to the development of a stress and not due to a chemical attack at the crack tip. The stresses must be derived from some chemo-mechanical process involving reaction between the glass surface and the environment. The resulting microcracks are sharp on a microscopic scale and drive into virgin glass. As fracture proceeds, the opportunity arises for secondary, tertiary etc. cracking from the undercuts known to exist at striations.

The crenellated striations formed by microcracks obviously differ from the usual features produced in the hackle zone of fracture surfaces, Johnson and Holloway (1966,1968). This, together with the irregular shaped crack front appears to suggest that the stresses which advance the crack tip are localised and internal, not simply applied at the site of the source flaw or uniformly distributed over the outer surface of the specimen.

The higher concentration of sodium found after longer exposure suggests that the stresses driving the cracks are associated with the incorporation of sodium. However, the mechanism by which sodium enters the glass network is not clear: the lack of potential exchange ions in silica glass

would seem to rule out any normal ion exchange process. The trace element content of the various fused silicas was small and in any case no systematic differences in the production of microcracks was detected for the range of glasses studied.

Comparison with the process used in the commercial production of chemically toughened glass raises a further interesting problem. The usual procedure relies on the exchange of relatively large ions for smaller ions in the glass, at temperatures just below the glass softening point, so that swelling and consequent compression occurs in the surface layers. At first sight this appears similar in principle to the mechanism suggested to account for spontaneous cracking in silica; so why does this toughening process not cause extension of the microcracks which must surely be present on the surfaces of the commercial samples?

It is interesting to note that cracking has been observed during some ion exchange processes when the exchange begins at too low a temperature, Fine and Danielson (1988). The high temperature used in the normal process will result in a small concentration gradient of the large ions and good penetration into the surface layers; not only is the final compression layer typically about 100 microns deep, much greater than the length of normal surface microcracks, but the compression through much of this layer will be developed without the introduction of a large stress gradient so that the tips of the shallow surface microcracks will not lie in a region of

large tensile stress at any time during the process. Thus it seems likely that an essential feature of the process responsible for the spontaneous crack propagation in silica observed in our experiments is the development of a shallow, and, or high-gradient compression layer in the course of the reaction with the alkaline solutions.

The obvious lack of suitable positively charged ions in the network of fused silica suggests that the incorporation of sodium must be accomplished by a more complex route than a simple exchange. One possibility is that water, after an initial penetration, then provides suitable exchange ions in the form of hydrogen or, perhaps more likely, hydronium, H_3O^+. The incorporation of water into silica has been discussed by Budd (1961) who offers a model that relies essentially on ionic attraction. For example hydrogen or hydronium act in a strongly electrophilic fashion, that is they attack the sites of negatively charged, oxygen atoms.

4.4 Some Quantitative Estimates

It is of some interest to attempt even a crude estimate of the scale of the interaction needed to cause crack propagation. Roberts and Roberts (1964) have presented measurements for the diffusion depth of water into silica glass at high temperatures. Assuming that the diffusion depth, d, is proportional to the square root of time:

$$d=\sqrt{Dt}$$

and that D, the diffusion coefficient, varies with temperature as:

$$D=D_0\ e^{-E/kT}$$

(E is the activation energy, T the temperature and k is the Boltzmann constant) we can scale their results to predict penetration depths for different times and temperatures. Even if sodium were entering the network independently, the penetration depths would be of similar order since the values of activation energy and D_0 are comparable.

These calculations yield a penetration depth of 5nm after 10 days at 80°C, but only 0.1 nm at 20°C - clearly the latter figure has no direct physical meaning, but may perhaps be taken to suggest that significant diffusion may not occur at room temperature and this would correspond to the noted absence of microcracking at this temperature.

Assuming that microcracks are driven by a mechanism which provides an internal pressure, an estimation can be made of the degree of swelling required to achieve the required critical pressure. From the measurements of spontaneous macroscopic crack extension the average crack speed over the first 48 hours in silica glass is about 10^{-9} ms^{-1} and the stress intensity required to propagate cracks at this rate is around $2*10^5$ $Nm^{-3/2}$, Weidmann (1973). For a circular crack of radius a under internal pressure in an infinite elastic solid, the stress intensity factor is given by:

$$K = P(\pi a)^{1/2} \qquad [1]$$

where P is the internal pressure in the crack, Rooke and

Cartwright (1976). As usual symmetry allows the same expression to be used for a semi-circular crack in an infinite elastic half-space.

The relative volume increase required near the crack to provide an internal pressure, P, can be expressed:

$$\frac{dV}{V} = \frac{P}{K_B}$$

where K_B is the bulk modulus of the material. Or, since $K_B = E/3(1-2v)$ as:

$$\frac{dV}{V} = \frac{3(1-2v)P}{E}$$

For a crack of radius of 1mm the pressure needed to produce the required stress intensity factor would be:

$$P = 4.5 * 10^{6}\ Nm^{-2}$$

and taking $E=7.4 * 10^{10}\ Nm^{-3/2}$ and v=0.17 (Thermal Syndicate Ltd.) we find:

$$\frac{dV}{V} = \frac{1}{10,000}$$

We take the model offered by Budd (1961) once again and suppose that the interaction with the silica network and positively charged ions occurs at the sites of bridging oxygens, then it is possible to estimate the number of such sites in the 5nm penetration layer estimated above. The Si-O-Si atomic separation is of the order of 0.32 nm, over one square metre of surface there are approximately 10^{15} sites and for a depth of 5nm, around $15 * 10^{15}$.

The incorporation of sodium into the surface layers evidently occurs at least as part of the overall interaction. Although normal soda-silica glasses have a higher density than pure silica, we can hardly expect long range rearrangements of the network at 80°C; moreover we do

not know what, or whether, other ions may be involved. So, to be consistent with our phenomenological model, we shall assume that each interaction with a bridging oxygen causes a local increase in volume.

Clearly plenty of oxygen sites are available in the surface layers of interest and a total average volume change of 1/10,000 could be achieved by local increases of, say, 10% at only 1 in every 1000 sites, or by only 1% if 1 in every 100 sites were involved.

These quantitative estimates, of course, do not have much significance, although it is perhaps fair to claim that the numbers obtained at least do not rule out the kind of mechanism for spontaneous cracking suggested above. Obviously there is need for further study, particularly for more sophisticated chemical analysis of specimens and monitoring of the solutions.

4.5 Conclusion

The mechanism responsible for the spontaneous cracking of fused silica immersed in these particular alkaline solutions is unclear. However, it does seem that the cracks begin from surface flaws, under the influence of mechanical stresses generated by reaction between the glass and the alkali; these stresses can become quite localised at a later stage. The reaction appears to involve the incorporation of sodium into the surface layers and this process is accelerated by the presence of the heavy alkaline ions in solution, but in an unknown manner.

In principle, the implications of this phenomenon of

spontaneous fracture for the long term durability of optical glass fibres may give cause for concern. Although the temperature dependence of the process, found in our simple investigation, and the improved quality of modern silica fibres offers some comfort, further experiments to establish the influence of both the concentration of sodium ions (?) and of likely contaminants over very much longer times might be of interest.

CHAPTER FIVE

INTRODUCTION

Reports that a variety of inorganic glasses could be indented by diamond pyramid indenters to leave permanent, crack-free impressions were made by Taylor (1949a+b). A discussion, following a paper given by the same author to the Society of Glass Technology (1950), clearly indicates that many other workers in the field of glass research at that period were sceptical of Taylor's claims for plastic flow in such an amorphous material at ambient temperatures. Since then further evidence has been presented that supports the ability of certain glasses to deform plastically, at least on a microscopic scale beneath indentations. However, the exact process of this deformation is still incompletely understood and the purpose of this section of the present thesis is to add further evidence for the microplastic behaviour associated with indentations.

Amongst the various features Taylor noted whilst indenting a range of optical glasses was the redistribution of material and the advent of cracking at higher loads. He suggested that the material immediately below the indenter was displaced to form a circular mound around the outsides of the inverted pyramidal impression. With greater loads, usually above 0.1 Kg, fractures commonly occured radiating from the four corners of the indent together with "subsidiary fractures" that isolated

the material surrounding the indent. These were to be identified later as the median/radial and lateral cracks respectively. Taylor illustrated the presence of a pile or mound of displaced material using optical interferometry. However, Peter (1970) provides an excellent scanning electron micrograph showing a similar feature surrounding an indentation made on Plate glass with a diamond pyramid of much sharper included angle (70°) between opposite facets.

Relationships between the hardness of materials and their ability to withstand surface damage such as indentation and scratching were quantified by Mohs in the early nineteenth century. He developed a scale based on the ability of ten chosen minerals to scratch each other, the extremes of this relative scale being talc (softest) and diamond. Another century passed before the ideas of such inflicted damage were standardised further. It was realised that penetrating or indenting a surface with a standard regular shaped indenter, made of a material harder than the range of test materials, left measurable impressions of sizes dependant on the load applied and the test material's "indentation resistance" or hardness.

Hence, "hardness numbers" were defined by either:

H.N. = load / actual area of impression [1]

or

H.N. = load / projected area of impression [2]

One such indentation test widely adopted by metallurgists was the Brinell test where a small steel ball is loaded on the test material. However, the hardness

number was found to vary with the applied load and indenter diameter. This inconsistency together with the testing limitations of the ball (no material harder than steel would give an impression - the ball would suffer damage) eventually lead to development of the Vickers Hardness test. During Brinell measurements it was noted that consistent results were gained whenever the load was such that the diameter of the indentation was 0.375 times the indenter diameter (Figure 5.1). For this condition it was calculated that the angle subtended by the tangent planes to the surface of the ball was 136° and this lead to the development of the Vickers Hardness machine comprising a diamond pyramid indenter of this included angle between the opposite facets. The results from such tests were subsequently named "Vickers Hardness Numbers" (VHN) and calculated by using an equation similar to [2] to give:

$$VHN = 2P \sin(\theta/2) / d^2 \qquad [3]$$

where P equals load, θ is the included angle and d the indentation diagonal.

(The latest convention is to express VHN in units of Nm^{-2})

Following Taylor's initial observations, correlations between hardness and other physical properties of glass were explored, and, following the lead of metallurgists, the hardness numbers of glasses were used to estimate flow stresses for these materials. No other method has been yet been found which provides an estimate of the flow stress for glass.

Ainsworth (1954) seems to be the first author to

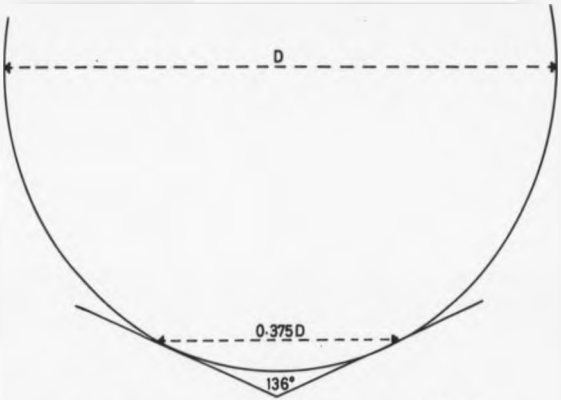

FIGURE 5.1 Conditions for which a ball indenter is equivalent to a pyramidal indenter, as found from Brinell test results.

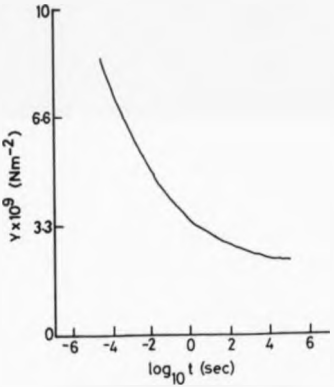

FIGURE 5.2 Plot of Yield Stress, Y, against $\text{Log}_{(10)}$ Time for soda lime silica glass at 20°C (after Marsh, 1964a).

obtain a value for the flow stress of glass, i.e. the threshold stress above which permanent deformation occurs. He argued that the effective tensile stress acting on the glass surface once in contact with the indenter could be resolved into components parallel and perpendicular to the area of contact. As the indentation proceeds the contact area increases to lower the value of this tensile stress until equal to that of the flow stress.

Then: $Y = \mathrm{Cos}(68°)H$

or

$$H/Y = 2.6$$

This compared favourably with the figure calculated by Tabor (1951) for metals of $H/Y \approx 3$.

Marsh (1964a+b) redirected the analysis of plastic flow in glasses and also questioned whether glass should be considered as an ideal brittle material. An essential characteristic of an ideally brittle material might be that the energy to cause fracture should be equal to the surface free energy - the energy required to rupture bonds between adjacent surface ions. Marsh used the fact that the fracture energy of glass exceeded its surface energy to argue a case for some form of plastic deformation not only beneath indentations but also at the tip of a crack during fracture. He made no attempt to describe the mechanisms of such deformation but did envisage flow taking place within a small zone at the crack tip. The fact that the pristine strength of glass (approximately E/20 where E is Youngs Modulus) was well above the flow stress deduced from the simple $H/Y \approx 3$ relationship although such specimens

exhibited no signs of macroscopic flow, lead Marsh to re-examine the H_ν/Y relationship.

Ainsworth (1954) postulated, essentially, a process of tangential flow away from the impression. Marsh (1964a+b) took a different view by proposing radial flow for highly elastic materials. Work by Samuels and Mulhearn (1957) had previously shown that contours of equal strain could be mapped out beneath Vickers indentations to form a series of concentric hemispheres. This radial distribution of strain was regarded by Marsh to be analogous to the stress distribution around an expanding cavity under an uniformly distributed internal pressure. By simplifying a spherical cavity solution previously calculated for the autofrettage conditions in pressure vessels and gunbarrels, Marsh deduced a relationship between hardness number and yield stress which took the form:

$$H_\nu/Y = C+KB\ln(Z) \qquad [4]$$

where $B = 3/(3-\alpha)$, $Z = 3/(\alpha+3u-\alpha\mu)$, $\alpha = 6Y(1-2v)/E$ and $\mu = Y(1+v)/E$. v is Poissons ratio, C and K are constants.

By plotting H_ν/Y against $B\ln(Z)$ (essentially a function of E/Y) for a wide range of materials with different, known values of Y/E, Marsh was able to verify the form of this relationship and to interpolate a value of $H_\nu/Y = 1.6$ for "typical glasses". It should be noted that for all the materials used in establishing equation [4], a value for the yield stress of each material, except glasses, was available from macroscopic compression tests.

Using the spherical cavity model, Marsh showed that the yield stress calculated from indentation hardness

measurements and the fracture stresses of pristine glass specimens in air correlated well for several glasses, loading times and temperatures. In the particular case of soda glass he also showed that the yield stress, calculated from H_v measurements, falls with increased loading time (Figure 5.2), although appearing to reach a constant value for loading periods greater than about 100 seconds.

Indications of structural changes beneath indentations were provided by Peter (1970) and allowed direct comparison with the hypothetical radial flow process developed by Samuel and Mulhearn (1957) and Marsh (1964a+b). To achieve this Peter adopted a method of sectioning indentations involving indenting near the tip of a pre-existing crack in the specimen so that the crack could be extended subsequentially to propagate through the indentation. This technique had previously been used in metallurgical studies by Samuels and Mulhearn (1957). The resulting "half-surface and section" views revealed a pattern of intersecting curved lines beneath the indentations and approaching the surface.

This sectioning method has since been used for the examination of indentation fracture and deformation by numerous authors. Hagan and Swain (1978) used the technique in a study which lead to a classification of the deformational features beneath Vickers pyramidal indentations in soda glass (Figure 5.3).

Indentations showed an approximately semi-circular zone, beneath the V-shaped profile of the indent, which appeared to be comprised of a series of intersecting lines.

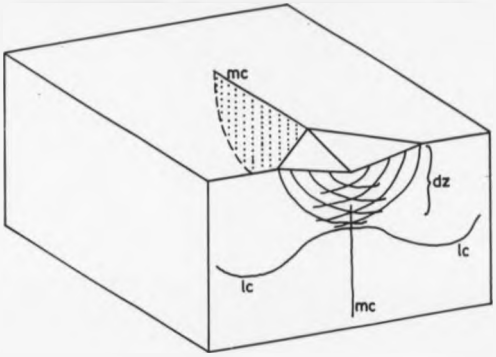

FIGURE 5.3 Schematic representation of the characteristic fracture and flow deformation beneath Vickers indentations on soda lime silica
mc = median crack lc lateral crack dz = plastically deformed zone

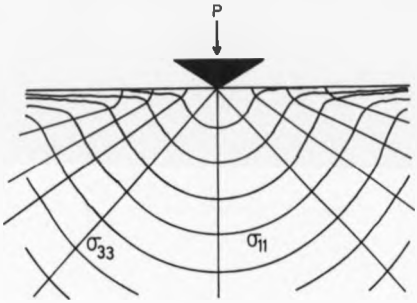

FIGURE 5.4 Sectional view of the principal stress trajectories σ_{11} and σ_{33} in a Boussinesq field beneath a point indentation on an elastic solid. (after Lawn and Swain, 1975). Poissons ratio = 0.25. σ_{22} is concentric about the point of indentation and on the indentation surface.

The orientations of the lines were noted as being similar to those of the elastic shear stress trajectories beneath point loads that had previously been calculated by Lawn and Wilshaw (1975). Figure 5.4 represents such maximum shear stress trajectories in the so called "Boussinesq elastic field" for an elastic solid under point loading. A value for Poissons ratio of 0.25 was used as a typical value for brittle solids which compares favourably to that of 0.21 for soda glass (Shand, 1958). The similarities between these stress trajectories, the strain contours of Samuel and Mulhearn (1957) and the experimentally observed orientation of lines in soda glass all implied a radial flow regime.

Characteristic features that had previously been recognised on indentation surfaces of soda glass as early as 1949 by Taylor, were now made visible in the sub-surface region by the sectioning method; Hagan and Swain (1978) were able to comment upon these 3-dimensional forms and their origin. With respect to Figure 5.3 the median crack, mc, was a penny shaped, semi-circular crack vertically beneath the diagonals of the pyramidal indentation, the surface traces of which are commonly seen radiating from the indentation corners. If loading is insufficient to develop the median cracks to a depth greater than that of the plastically deformed zone, dz, they are confined to the near surface and are then of the form often refered to radial cracks. Hagan and Swain noted that the origin of the median crack was usually found within the plastically deformed zone and often at the intersection of the shear

directly beneath the apex of the indentation profile. Lawn and Fuller (1975) and Lawn and Swain (1975) had previously described the initiation and propagation of median cracks beneath sharp or pointed indenters such as Vickers pyramidal indenters. Both reports envisaged crack nucleation directly below the indenter point where the greatest stress occurs and the nuclei are "created by the deformation process". The relationship between the median crack origin and the intersecting flow lines found by Hagan and Swain (1978) supported the idea that the deformation process played a role in crack nucleation.

The median crack, sometimes refered to as the "median vent", extends downwards into the bulk during the loading half-cycle, progressing to greater depth with increasing load. Upon unloading, the crack closes but does not heal. The lateral cracks, lc in Figure 5.3, are relatively large, saucer-shaped cracks below and roughly parallel to the indentation surface. When well developed, they tend to turn towards the surface at their extremities. Hagan and Swain (1978) considered these to initiate at favourable sub-surface flaws at the elastic/plastic boundary at the base of the deformed zone, dz. But it is clear that they propagate exclusively during the unloading half-cycle under the relatively high tensile stress set up as the elastic strains around the deformed zone attempt to relax.

The features described above are characteristic of the deformation associated with indentations on what have become known as "normal" glasses. This classification of glasses according to particular physical properties was

originally made by Anderson and Diennes (1960). They recognised that fused silica in particular, possessed "anomalous" properties compared to crystalline materials. The four main anomalies were the temperature dependence of the elastic modulus, the refractive index and the thermal expansion coefficient, and the variaton of compressibility with pressure.

Arora et al (1979) illustrated that the normal and anomalous glasses also produced distinctive but differing forms of sub-indent deformation. Whereas normal glasses such as soda-lime-silica showed signs of shear in the form of an intersecting line pattern, anomalous glasses, of which fused silica is now regarded as the archetype, gave Hertzian type fractures with no apparent signs of accompanying shear deformation.

Figure 5.5 illustrates the Hertzian type fractures associated with Vickers indentations on fused silica. The dominant fractures are the cone cracks (cc). These propagate during loading, nucleating around the periphery of the indentation as ring cracks then extending down and outwards from the indenter as further load is applied. As deformation progresses, the surface trace of the cone crack becomes enveloped within the expanding contact area until eventually a new ring crack initiates at the new periphery leading to a series of steeply dipping cone cracks. Median and lateral cracking may accompany the cone cracks, but the cone cracks usually remain dominant.

The different forms of deformation associated with indentations on the two types of glass could imply that

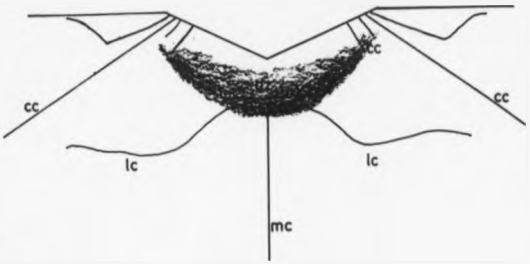

FIGURE 5.5 Schematic representation of the characteristic features beneath Vickers indentations on Fused Silica. mc = median crack cc = cone crack lc = lateral crack dz = zone of densification.

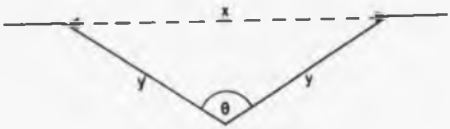

FIGURE 5.7 Calculation of the maximum surface strain beneath pyramidal indenters of included angle θ.

$$\% \text{ strain} = \operatorname{cosec} \theta/2 \times 100 = \frac{2Y}{x} \times 100$$

For the indenters used in this study:

$\theta = 125°$, $\varepsilon = 12.74\%$
$\theta = 136°$, $\varepsilon = 7.85\%$
$\theta = 150°$, $\varepsilon = 3.53\%$

different mechanisms may be responsible for their production and hence that the process of crack initiation may be different in normal and anomalous glasses. If this were so, then presumably the different behaviour is somehow related to the molecular arrangement in these materials.

A widely accepted model for the structure of silicate glasses was presented by Zachariasen (1932) who proposed an extended network of randomly orientated SiO_4 tetrahedra and this idea found support in the later X-ray analysis by Warren (1937). A schematic illustration of the random network structure of glass is included in Figure 5.6 . Fused silica could be formed by a basic network of SiO_4 tetrahedra whereas "modified" glasses such as soda glass would need to accommodate "network modifying ions" such as Na^+, Ca^{2+} and Mg^{2+} within the open network.

Alternatives to the Zachariasen and Warren model have been suggested including that proposed by Randall et al (1931) based on the aggregation of crystallites with random orientation to leave no long range order. More recently Goodman (1986,1987) has presented a model of "strained mixed clusters" which relies heavily on phase separation and polymorphism. Whichever model is accepted, however, the role of the network modifiers seems central to the different deformation processes.

There is some direct evidence to suggest a transition in the deformation process from densification to shear flow as modifier ion content is increased. Ernsberger (1968) detected an increase in refractive index within the deformed zone beneath indentations in fused silica and

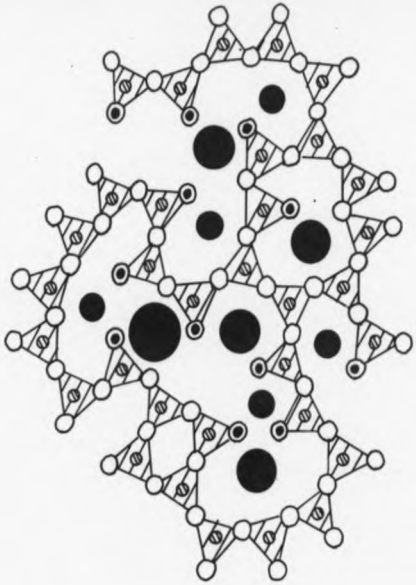

FIGURE 5.6 Two dimensional representation of the random network model of glass structure. For Soda lime silica glass the network modifiers are sodium, calcium and magnesium. Fused silica is essentially a similar network of silicon-oxygen tetrahdera with the absence of modifying ions.

attributed this to densification, i.e. a compaction of the network structure. Neely and Mackenzie (1968) found larger scale, permanent compaction of fused silica under "hydrostatic" compression. Subsequently, Peter (1970) demonstrated that the tendancy for material to pile up around indentations increased with increase in the network modifier content. The dominance of such shear flow in normal glasses implies that modifying ions in some way provide an easy slip path through the rigid, stongly covalent network of SiO_4 tetrahedra, Hagan (1980), whilst at the same time restrict any closure or compaction of the network.

Most of the details concerning the indentation deformation of various glasses hitherto reported relate to effects observed with Vickers indenters with an interfacial angle of 136°. The Vickers indenter imparts a maximum surface strain of approximately 8% (Figure 5.7) and, arguably, this may have different consequences for glass with different intrinsic failure strains. For instance, at 8%, the surface strain imposed by Vickers indenter is greater than the maximum tensile elastic strain at failure for pristine specimens of soda glass, approximately 6%, but it falls well below that which can be sustained by fused silica, approximately 12% at liquid nitrogen temperatures (Mallinder and Proctor, 1964).

A study of the influence of surface strain, determined by the indenter included angle, was therefore chosen as a basis for this section of the present thesis. In particular, would increasing the suface strain inflicted on

fused silica to over 12% promote shear deformation in that material? To achieve this increase in strain a "sharper" indenter i.e. with a smaller interfacial angle was used in the experiments to be described below. On the other hand, would a "blunt" indentation on soda glass, producing a surface strain of less than 8%, give Hertzian type fracture and no longer give rise to shear lines? The forms of the resulting deformation would be of interest, especially any information that could clarify the nature of the flow lines and their intersecting pattern.

5.1 Terminology

Before entering into an account of the experimental techniques and corresponding results it is convenient here to define some of the important terms that will be employed. Any mention of "plastic deformation" will be made with its general connotation in mind, i.e. any permanent deformation that is not recovered elastically. As pointed out by Ernsberger (1968) this term can then encompass the shear flow common in metals and perhaps normal glasses together with the densification or compaction effects which seem to occur in fused silica.

The lines that constitute the intersecting pattern found beneath soda glass indentations will be termed "flow lines" in common with most previous reports. This term is considered applicable as it does not necessarily presume a particular mechanism.

Fractures will be described according to Figures 5.3 and 5.5 for soda and fused silica glass respectively. When

describing the indentation form the terms used will be as illustrated in Figure 5.8.

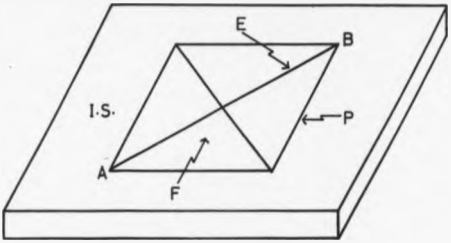

a) I.S. = Indentation Surface E = Pyramidal periphery
F = facet

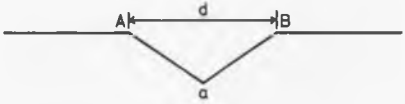

b) Section through AB
d = indentation diagonal a = apex

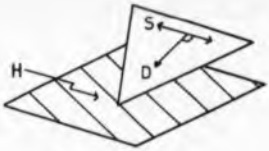

c) Facet orientation
H = Horizontal plane S = Strike D = Dip

FIGURE 5.8 Terminology to be used throughout this thesis to describe pyramidal indentations.

CHAPTER SIX

EXPERIMENTAL METHODS

6.1 Introduction

Indentation experiments have been carried out on two types of glass at two different temperatures using diamond, pyramid indenters with three different included angles. Some indentations were produced so that sections could be examined.

This chapter describes the apparatus and procedures used for indenting specimens as well as etching techniques, used to enhance structural detail around the indents. An appraisal is given of the sectioning technique for revealing sub-indent structure.

6.2 Materials and Preparation

In this study, two different types of glass have been used: a soda-lime-silica, (Float glass, Pilkington Bros. Ltd.) and a fused silica, (Thermal Syndicate Ltd.). The compositions and selected technical information are given in Table 2.2.

Batches of samples were cleaned in an ultrasonic bath for ten minutes with a 10% solution of Decon 90 (Decon Laboratories Ltd.) in distilled water. They were then rinsed with distilled water, dried in a warm air cabinet and stored in covered petri dishes.

6.3 Indentation Apparatus

Indentations were made by using two different machines: for loads less than 2 Kg a micro-indenter based on a design by Gunasekera (1970) was used. However, for greater loads a commercial microhardness indenter designed for use with the Vickers Projection Microscope proved essential because of its superior stability with higher loads.

The three pyramidal diamond indenters were cut to the required included angles (125°, 136° and 150°) and supplied mounted on mild steel rods by Star Industries Ltd. .

The Gunasekera type apparatus is illustrated schematically in Figure 6.1. A balancing arm carrying the indenter and the load is pivoted on a steel knife edge supported in a V-grooved brass block, in turn mounted on a baseplate with the centre machined out. This plate could be clamped onto the stage of the Vickers microscope and with a specimen resting on a glass slide, 1-2 mm thick depending upon the intended load, the indentation process could be viewed from below once the load was applied. A simple screw through the baseplate can be used to support the pivotted arm and facilitates specimen loading and unloading.

For loads greater than 2 Kg a Cooke, Troughton and Simms (CTS) microhardness tester, adapted to accommodate the various types of indenter mount, was used. With this device the specimen is held on the pivoted arm which also carries the load and is supported on the stage of the Vickers microscope, while the indenter is mounted in the

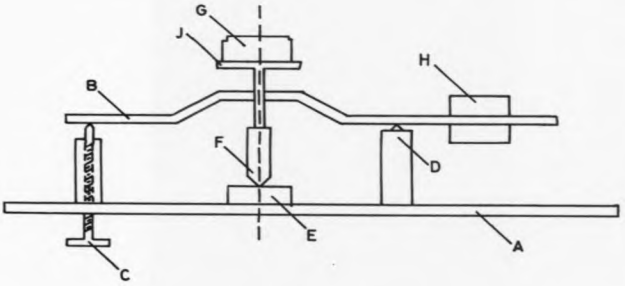

FIGURE 6.1 The Gunasekera type indentation apparatus

KEY: A = Base plate B = Balancing arm C = Loading/unloading screw
D = Supporting/pivotted block E = Specimen F = Indenter
G = Load H = Counter balance J = Loading platform

objective holder. The indenter and specimen are brought into contact by adjusting the focusing controls of the microscope. For indentations with a 136° diamond pyramid a commercial objective with a small diamond mounted on the front lens was available (CTS Ltd.), but for the other indenters a brass holder was made which could be mounted in the objective carrier (Figure 6.2).

For indentations at high temperature, a tester designed by Stavrinidis (1980) was used after minor alterations. A cavity, within an asbestos block was heated by two 65 watt soldering iron elements, the temperature being controlled to $\pm 2°$ by a Transitrol (type 994) temperature controller (Ether Ltd.). A maximum temperature of 670° Kelvin was achieved with this apparatus.

6.4 Indentation Methods

Sectioned indentations were produced by indenting a specimen near the tip of a preformed crack and then, subsequently, propagating the crack through the whole length of the specimen. Strips of glass between 1.5 to 2.0cm wide were cut from the stock material. A crack, approximately 1.0 cm long, was propagated along the mid plane from one end of the strip by gently tapping on the reverse side of a diamond score. An individual sample approximately 2.0 cm square was produced by then sectioning the strip about 1.0 cm ahead of the crack tip. Samples with curved or twisted cracks were discarded.

Positioning the indenter so that it straddled the line

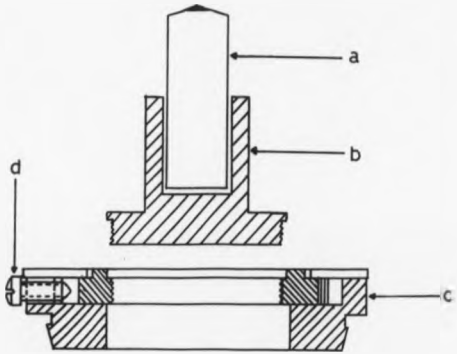

FIGURE 6.2 Diagram of the holder designed to accept mounted diamond indenters for use with the CTS indentation apparatus on the Vickers projection microscope.

a = mounted indenter
b = brass holder
c = CTS objective holder
d = centring screw

of the crack near the tip was simplest with the CTS tester and the 136°, Vickers diamond mounted on its objective lens. Even in this case however, several indentations were usually needed with re-adjustment of the specimen position after each attempt in order to place the indenter accurately across the line of the crack and near the tip. (The particular problems of indent positioning with respect to the crack tip are discussed later in this chapter).

Two different orientations of the pyramidal indenters with respect to the preformed crack were employed: such that the diagonal of the indentation, corner to corner, lay parallel or at 45° to the crack (Figure 6.3). The first orientation is that favoured by Hagan and Swain (1978), Hagan (1979a+b, 1980) and Hagan and Van der Zwaag (1984). Providing the centre of the indentation lies on the crack the sectioning plane coincides with that of the median crack which commonly accompanies pyramidal indentations in soda-lime-silica glass to give a "lateral" section. The latter orientation, as used by Dick (1970) and Hagan (1979a) is commonly described as the median plane.

The loading rate was constant at approximately $7*10^{-5}$ ms^{-1} and the duration of loading was normally 20 seconds. Unsectioned indents could be made with either type of apparatus fixed to the Vickers microscope or with the Gunasekera tester on a laboratory bench.

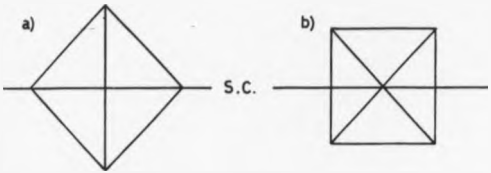

FIGURE 6.3 Orientation of indentations with respect to the Sectioning crack (s.c.) a) lateral section or b) Median section.

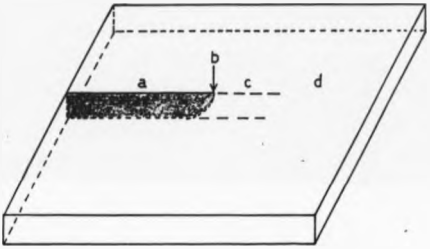

FIGURE 6.4 The four possibilities for indentation position with respect to the preformed sectioning crack
a) Open crack, b) Apparent crack tip
c) Healed crack or d) "Virgin" glass.

6.5 Appraisal of Indentation Sectioning

Since the adoption of the sectioning method for use with glass, only Hagan and Swain (1978) appear to have investigated the relationship between indenter position with respect to the preformed crack and the subsequent sub-indent structural damage. However, they were concerned with spherical indenters and no similar results for pyramidal indenters are known, hence such observations were made during this study.

As described, each specimen intended for the sectioning process was cracked part way along its mid-plane. This crack was then liable to heal; in practice some part remains open, often due to debris wedging the crack walls apart. Any healed portion requires a finite strain energy release rate for repropagation, G_r, which upon aging or annealing, increases to approach that required for the slow propagation of cracks in virgin glass, G_v, Stavrinidis (1980). As the test specimens were cleaned after pre-cracking, including a period in a warm air cabinet, and at least 24 hours elapsed before any indentations were made on them, any healed cracks could be considered as well-aged, i.e. $G_r \lesssim G_v$. (Further details of crack healing can be found in Chapter One of this thesis).

Confusion over the position of indentations with respect to the preformed crack exists in past reports. This author recognised four possibilities, compare Figure 6.4:

a) Open Crack

Here the crack walls are separated and the crack opening is microscopically visible.

b) On The Apparent Crack Tip

This is the boundary between the visibly open crack and a healed portion.

c) Healed Crack Position

Here previously separated crack walls have adhered together to leave little or no visible trace of crack opening. Upon loading, these portions become visible by re-opening either side of the indentation and this has the effect of advancing the "apparent" crack tip.

d) On "Virgin" Glass

This is ahead of any cracking whether now open or healed.

In the present series of experiments it became clear that the quality of indents made on an open crack, i.e. (a) above, varied according to their displacement behind the apparent tip. Those well behind the crack tip rarely left clean, intact impressions; instead the specimen edges tended to shatter (Figure 6.5a+b). Closer to the tip, however, the resulting indent sections were usually intact and showed sub-indent patterns, although the features of the lateral or median cracking and the "flow line field" on opposite sections of a single indent did not match, Figure 6.6a+b).

Indenting on a healed portion of a crack gave results similar to those for an open crack close to the apparent

Figures 6.5a and 6.5b

Sections of a 125° indentation on soda-lime-silica made under a load of 19.6 N and well behind the apparent crack tip, illustrating the broken nature of the section.

Scales: top 1mm=6.25μm

bottom 1mm=1.25μm

Figures 6.6a and 6.6b

Non-matching sections from a single 125° indentation made on soda-lime-silica under a load of 19.6 N and on an open crack closely behind the apparent crack tip.

Scales: both 1mm=1.25μm

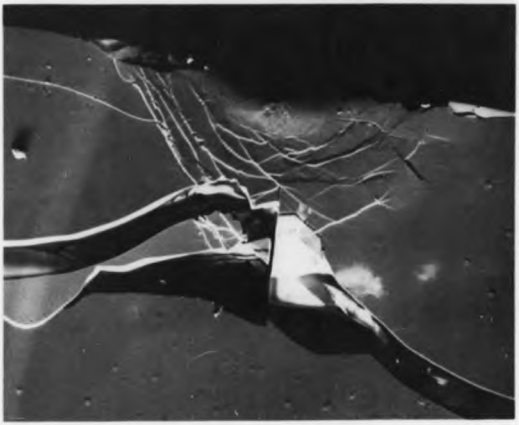

tip. Again the features on opposing sections did not totally match.

Clean, intact sections of indentations made on "virgin" glass were never produced. Either the indenter was positioned too far ahead and so missed the path of the sectioning crack or the indents shattered on sectioning.

In summary, indentations made on an open crack (close enough to the crack tip to restrict crack wall separation) and on healed portions gave the best sections, with no differences in the general form of the sub-indent deformation. A position on the apparent crack tip gave satisfactory results except when healing was absent ahead of the tip, in which case the crack was often deflected off course as it dissected the indent, causing it to shatter. No variation in the deformation pattern was found with the indenter position, within the limits set above, therefore comparisons with results of past authors can be made, despite their vague specification of indenter positioning.

6.6 Etching of Indentations

Etching was used to enhance the detail of structures within the surface or in some cases to uncover underlying features. Indentations were always examined with an optical microscope or a scanning electron microscope (SEM), prior to any etching.

The etchant used throughout the study was a 5% volume mixture of hydrofluoric acid (40%) to distilled water. Two etching techniques were used:

a) **Single Etching**

Specimens were immersed for a single continuous period before washing with distilled water.

b) **Progressive Etching**

Specimens were immersed for short, consecutive periods, each stage being followed by washing, drying in warm air and microscopic examination, thereby building up a series of images of the "progressive" etching history.

The preparation of specimens for SEM viewing included the deposition of a thin layer of gold onto the surface. However, this did not restrict subsequent etching as the gold was easily removed upon immersion in the etchant to leave the underlying glass subject to attack.

CHAPTER SEVEN

INDENTATION RESULTS

7.1 Introduction

In the present chapter the results obtained by indenting soda glass and fused silica glass under various experimental conditions are described. The majority of the results are of a qualitative nature - in the form of electron or optical micrographs and schematic diagrams. However, some quantitative hardness results are included.

Results for the two glass compositions will be presented separately. Initially, micrographs representing results from selected test conditions will be described in a manner as neutral and objective as possible. This will then be followed by preliminary discussions comparing the visible features with those described in previous reports, or by a detailed analysis of the features believed to be original to this study.

In the light of the present experimental programme a re-appraisal of the problems of indentation sectioning is included.

The significance of the results to possible deformational processes in glass will not be of great concern here but will be included in the final discussion in Chapter Eight.

7.2 Soda-lime-silica Glass

The scanning electron micrographs Figures 7.1a and 7.1b are the lateral and median sections respectively of

Figure 7.1a

Lateral section of a Vickers 136° indentation on soda-lime-silica under a load of 19.6 N.

Scale: 1mm=1.25μm

Figure 7.1b

Median section of a Vickers 136° indentation made on soda-lime-silica under a load of 19.6 N .

Scale: 1mm=1μm

different 136° Vickers indentations made under a load of 19.6 N.

Figure 7.1a reveals a shallow, V-shaped indentation profile and immediately beneath it, an approximately semi-circular area delineated by a pattern of curved, almost concentric, intersecting lines. These lines appear quite different from the cracks, which can be seen to be open or to cast obvious shadows where relative displacements have produced steps. The lines also intersect at angles other than 90°, which is usually not the case for fractures. Below the apex of the profile is a vertical crack extending from within the area of the line pattern into the bulk. Wing-shaped cracks extend from the region near the base of the line pattern to either side of the indentation. A number of shorter cracks can be seen, confined in general to the area of the line pattern and with a radial orientation with respect to the profile apex.

Figure 7.1b shows similar features but now in the median plane. The walls of the V-shaped profile are now inclined at a steeper angle and the base is slightly flat. Although the line pattern remains similar to the lateral section, differences in the cracking can be recognised. The single vertical crack beneath the apex is now replaced by two cracks. One of these turns into, the other intersects, basal cracks that extend approximately parallel to the free surface to either side of the indentation. The wing-like cracks are repeated but there are no short radial cracks within the line-patterned area.

All the features noted in Figures 7.1a and 7.1b can be

readily identified with those reported by several authors for Vickers indentations. The intersecting lines are the flow lines (fl) the extent of which define the semi-circular deformed zone (dz) and are commonly attributed to a shear process. The vertical cracks are the traces of median cracking (mc). Only one median crack is seen in Figure 7.1a because in this orientation its orthogonal counterpart has been used as the sectioning plane. The presence of two median cracks in Figure 7.1b can be attributed to the fact that the sectioning plane is slightly off the centre of the indentation. The flat base to the profile also supports this interpretation.

The horizontal base or "skirt" to the median cracks in Figure 7.1b is a consequence of the tensile stresses which arise during unloading. This is also the case for the wing-shaped cracks that have previously been noted as lateral cracks (lc). Finally, the short cracks found within the deformed zone were reported by Hagan (1980) as the result of secondary radial cracks (src) which initiate and propagate during the loading half cycle.

7.3 125° and 150° Indentations

In general the structures found beneath 125° and 150° indentations on soda glass were similar to those associated with 136° Vickers indentations.

Figures 7.2 and 7.3 show 125° and 150° indentations, respectively, under 19.6 N load and sectioned in the lateral orientation; both show a V-shaped surface profile beneath which there is an approximately semi-cicular

Figure 7.2

Lateral section of a 125° indentation made on soda-lime-silica under a load of 19.6 N .

Scale: 1mm=1.04μm

Figure 7.3

Lateral section of a 150° indentation made on soda-lime-silica under a load of 19.6 N .

Scale: 1mm=1.25μm

deformed zone consisting of an intersecting pattern of curving lines. Lateral cracking has occurred with both these indentations but only the 125° example exhibits a median crack. Although not unusual under these loads, the absence of median cracks beneath 150° indentations was not typical.

Despite the overall similarities between the patterns beneath 125°, 150° and Vickers indentations, close examination reveals interesting differences between the three conditions and these will be discussed in the following sections.

The distinction between cracks and flow lines is clear at high magnification. Figure 7.4 is an electron micrograph of a part of the deformed zone of a 150° pyramidal indentation produced under a load of 2.94 N. As already mentioned, the flow lines intersect at oblique angles whereas one crack usually meets another at 90° and does not cross it. Another significant feature, is the kinking of flow lines (k) at the intersections. If the "flow line" is interpretted as the outcropping on the plane of the section of a shear surface, then the kinks can provide an an estimate of the relative shear movement along the surface. From Figure 7.4 a maximum kink length of 0.4 microns was found and this compares favourably with the figure of 0.5 micron reported by Hagan (1980).

Figure 7.5 illustrates the median section of a different 150° indentation, made under a similar load. Towards the top of the electron micrograph the indentation profile is seen. Two cracks run approximately horizontally

Figure 7.4

Part of the deformed zone beneath a 150° indentation made under 2.94 N load on soda-lime-silica. Examples of flow line intersection kinks are marked "k".

Scale: 1mm=0.06μm

Figure 7.5

Part of the deformed zone beneath a 150° indentation made under 2.94 N load on soda-lime-silica. The indentation profile is to the top of the picture. Two main flow lines (l) confine a region of finer scale flow lines (fl).

Scale: 1mm=0.05μm

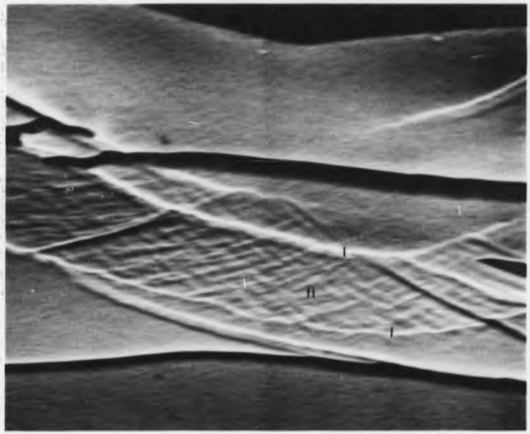
I
II
I

across the picture; the bright 'edges' and the shadows imply that there is a step in the sectioned surface associated with each crack presumably caused by displacement parallel to the crack surfaces and towards the plane of the section. Between the two cracks, a pair of curving lines (l) almost concentric with each other, define a band of material within which extremely fine-scale intersecting lines (fl) are seen. These very fine scale lines appear to intersect at oblique angles similar to the flow lines previously discussed. Hence, for the 150° indenter at least, flow lines on different scales appear possible. The width of the band between the two lines marked (l) is approximately 1.2 micron and between the fine scale lines is approximately 0.1 micron. The presence of fine scale flow lines between more prominent lines was observed only on this specimen, however, a gradation in the spacing of lines was often apparent for all three indenters. Figure 7.2, a 125° pyramidal indentation at 19.6 N load, illustrates this well. No flow-line detail can be seen immediately below the profile apex yet out towards the extremities of the deformed zone, distinct flow lines are visible. Kinking occurs on these lines and the spacing between concentric lines is approximately 5 micron.

Some of the features which lie beneath indentations and are exposed by the sectioning procedure, appear to give rise to marks on the indentation surface itself, within and immediately surrounding the contact area. Figure 7.6 is of a 125° indentation at 2.94 N; the electron micrograph was taken with the specimen at 45° to the detector to give a

Figure 7.6

Half surface and section view of a 125° indentation made under a load of 2.94 N on soda-lime-silica. The specimen has been etched for 20 seconds.

Scale: 1mm=0.3μm

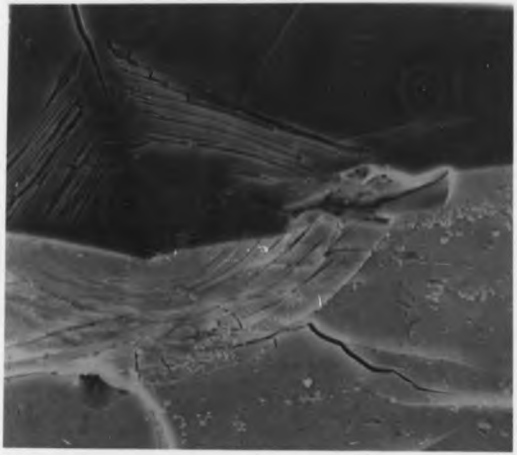

"half surface and section" view. This specimen had been etched for 20 seconds. The facets on the indentation surface show a series of lines, enhanced by the etching, running parallel to the strike direction. The outermost of these lines coincides approximately with the indentation periphery. Beneath the indentation on the sectioned plane is the semi-circular deformed zone containing an intersecting pattern of flow lines. A connection between the flow lines of the sectioned plane and the lines on the indentation surface facets is visible towards the right hand side of the indentation where the specimen edge has broken away. Such surface lines have previously been described as cracking by Bruche and Poppa (1956), and later by Holland (1966) in a description of an indentation produced by Bruche. The surface lines as demonstrated by Figure 7.6 clearly serve as indicators of the presence of flow lines beneath indentations. Hence it is suggested that unsectioned indentations can be used to infer information on subsurface deformation and helps overcome any reservations one may hold about evidence obtained from sectioned indentations.

Figures 7.3 and 7.7 illustrate the lateral and median sections respectively of two separate 150° indentations under a load of 19.6 N. As expected, the V-shaped indentation profiles are shallower than in the corresponding sections of a Vickers indentation. Both sections of the 150° indentations show a pattern of flow lines within a semi-circular zone, although there appears to be fewer lines for the 150° compared with the 136°

Figure 7.7

Median section of a 150° indentation made under a load of 19.6 N on soda-lime-silica.

Scale: 1mm=0.95μm

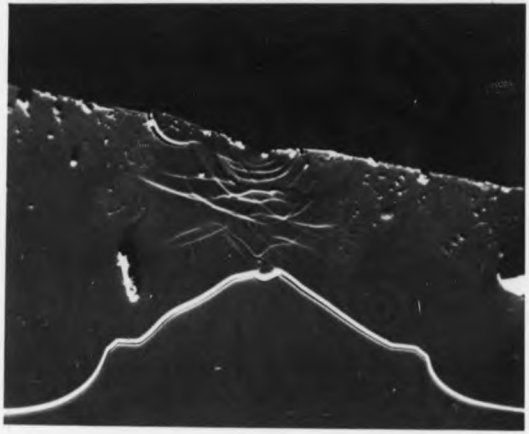

indentations. Extensive, wing-shaped lateral cracks are again found below the deformation zone. Although the particular samples illustrated in Figures 7.3 and 7.7 show no obvious median cracking, as previously mentioned, many 150° indentations do have such cracks associated with them. Secondary radial cracking is not present; however, within the deformed zone, to either side of the the indentation in Figure 7.3 and to the left hand side of Figure 7.7 , there are cracks roughly parallel to the indentation profile which outcrop at the surface near the lateral extremities of the deformed zone. These cracks give the appearance that portions of the indentation surface are being lifted away.

7.4 Unsectioned 150° Indentations

A series of 150° indentations was made on uncracked specimens without the intention of sectioning. A load of 49 N, relatively high for this study, was used to produce indentations large enough to permit optical examination to complement scanning electron micrography. Progressive etching was employed on the indentations and the application of this technique together with the resulting features are believed to be original to this study.

A single 150° / 49 N indentation in transmitted and reflected light respectively, is illustrated in Figures 7.8a and 7.8b . Both views reveal sharp indentation diagonals that define the extent of the contact area. Within the indentation periphery there are four or five distinct lines running parallel to the strike on each facet, and these are better seen in transmitted light. On

Figure 7.8a

Unsectioned and unetched 150° indentation made on soda-lime-silica under a load of 49 N. Transmitted light.

Scale: 1mm≡1.5μm

Figure 7.8b

As above but reflected light.

the other hand, reflected light reveals complications in the line pattern near the pyramidal edges. Within the area bounded by the innermost line, the transmitted view shows virtually no detail other than the indentation diagonals, but reflected light shows features in this area although on one facet only. The original colour photomicrographs revealed two sets of coloured interference fringes, a broad set running approximately along the facet strike and a much finer set meandering across the facet and overlapping the broad set in places. Interference contrast was also associated with the facet line patterns.

This specimen was progressively etched using immersions of 1 second. Photomicrographs 7.9a and 7.9b are the images in transmitted and reflected light of the sample after the first etch. Similar detail and corresponding interference patterns are still apparent on each facet and a central island, near circular in plan view, is now visible around the indentation apex. In transmitted light especially, striation-like marks are now seen near the pyramidal edges. The central island retained its form after four immersions in the etchant, as seen in Figures 7.10a and 7.10b, and the indentation apex remained sharp. Interference fringes are still seen in reflection while transmitted light again reveals most detail due to a lack of flaring. An area that takes the shape of a Maltese cross surrounds the central island; the recesses at the corners of this area show the complexity of the facet line pattern bordering the pyramidal edges. The number of lines on each facet has been increased by the appearance of new lines

Figure 7.9a

Same unsectioned 150° indentation as previous figure, now etched for one second. Transmitted light.

Scale: 1mm=1.5μm

Figure 7.9b

As above but reflected light.

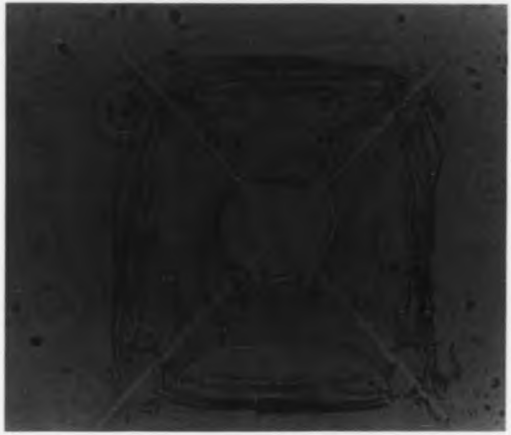

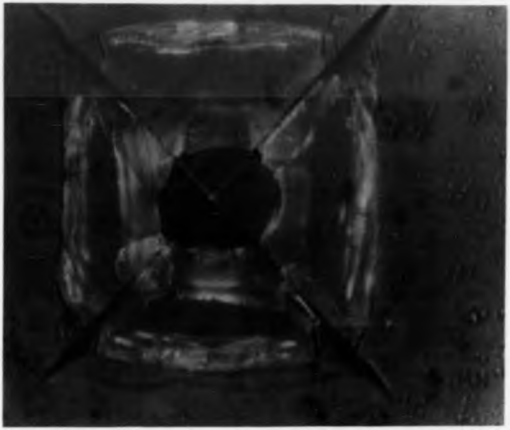

Figure 7.10a

Same unsectioned 150° indentation as previous figure, now etched for a total of four seconds. Transmitted light.

Scale: 1mm=1.5μm

Figure 7.10b

As above but reflected light.

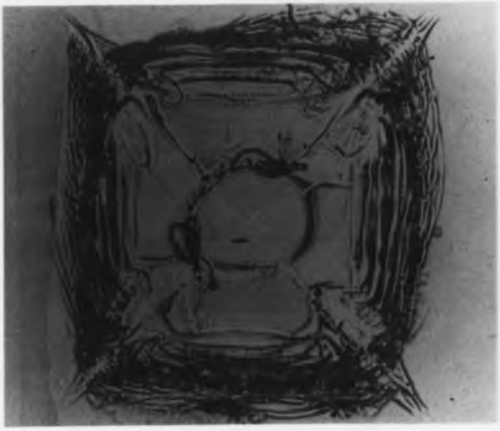

mainly towards the indentation periphery. After the fifth etch no new features were visible and so the sequence was completed with a continuous etch of 20 seconds. Shadows formed in transmitted light by the median cracks were first seen at this stage. It is not clear whether these cracks were present beforehand but required this longer etching to make them visible, or whether they are a new feature formed as a result of the etching, i.e. due to stress redistribution as material was removed by etching.

Scanning electron micrographs were taken at this stage to establish the topography of the etched surfaces. Figure 7.11 is a view taken at 45° to the indentation surface, the bottom of the frame being closest to the detector. The three zones distinguished optically, i.e. the outer facet lines, Maltese cross and central island, can all be readily identified. The central island is now seen to be raised above its surroundings to form a pedestal. The top of the pedestal still exhibits the indentation apex with no obvious signs of selective etching, while the pedestal walls dip sharply (by approximately 30 to 40°) to merge into the flatter, Maltese cross area. Large portions of the latter are free of any detail but in areas which, prior to etching, corresponded to the pyramidal edges, tongue shape grooves spread down towards the indentation centre. Finer detail of these tongues as they coalesce with the central pedestal is revealed by Figure 7.12 and some of the marks appear similar to the striations found on fracture surfaces of glass. This figure also shows the structure within the facet lines and at the former pyramidal edges. The tongues

Figure 7.11

Scanning electron micrograph of a 150° indentation made under 49 N load on soda-lime-silica. The specimen is tilted at 45° to the viewer. Total etching time 25 seconds.

Scale: 1mm=0.83μm

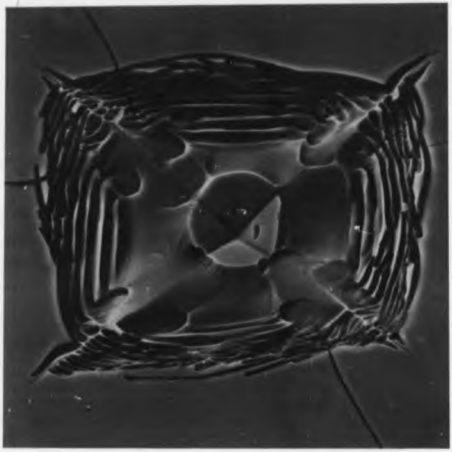

Figure 7.12

Scanning electron micrograph of a 150° indentation made under 49 N load on soda-lime-silica. The specimen is tilted 45° towards the viewer.

Detailed observations of structures in the region of the former pyramidal edge. Total etching 25 seconds.

Scale: 1mm=0.5μm

appear to be connected with the interaction of lines from adjacent facets and seem to be repeated for the successive flow lines.

Within the troughs formed from the facet lines during etching are a series of fine ridges parallel to the facet dip and therefore presumably to the direction of shear displacement over the flow surface.

The material comprising the pedestal is obviously more resistant to etching than that surrounding it. To explore this central material 150° indentations were made at loads low enough to produce a contact area less than that of the pedestal surface area in Figure 7.11 etc.. Figure 7.13 is an electron micrograph of a 0.294 N indentation etched for 20 seconds. The average diagonal length is approximately 10 microns, roughly half the diameter of the pedestal in the high load indentation. No flow line traces are visible even after etching the sample. Instead the facets appear to show slight pitting. Apparently, a permanent indentation has been made without the formation of the usual well-spaced flow lines.

The formation of such central regions at high load, or of a low load indentation devoid of flow lines after etching, were never obtained with Vickers or 125° indenters on soda glass.

Indentations at elevated temperatures were made in an attempt to compare the flow line features with those seen at laboratory temperature. A 150° indentation made under a load of 9.8 N at 293°K is illustrated in Figures 7.14a (unetched) and 7.14b (20 second etch). These may be

Figure 7.13

Scanning electron micrograph of a 150° indentation made under 0.294 N load on soda-lime-silica. Total etching 20 seconds.

Scale: 1mm=0.14μm

Figure 7.14a

Unetched 150° indentation made under 9.8 N load on soda-lime-silica at 293°K .

Scale: 1mm=0.42μm

Figure 7.14b

As above but after 20 seconds etching.

compared with Figures 7.15a and 7.15b which are the corresponding micrographs of an indentation made at 573°K with a similar load. A greater number of flow lines is apparent, even prior to etching, on the surface indented at high temperature; etching does not produce the central pedestal common at laboratory temperature and flow lines occur on the facet surface much nearer to the apex.

7.5 Hardness Measurements

Measurements of hardness number (H.N.) were made, using the Vickers, 125° and 150° indenters in turn at laboratory temperature.

All values of H.N. were calculated using the expression:

H.N. = load / projected area

(Equation [2], Chapter Five) from measurements taken using the CTS equipment on the Vickers projection microscope. Each experimental point represents a hardness number calculated from an average figure of d, the diagonal length, for at least three indentations (six diagonal measurements). Errors were estimated from the variation in d at a given load. The greatest scatter in values of d (up to $\pm 6\%$) was found at low loads, with the rather blunt impressions left by the 150° indenters.

Figure 7.16 gives the results for Vickers indentations together with some results by previous workers who used a similar range of load. Prod-Homme (1968) and Gunasekera (1970) both found a fall in H.N. at low loads and this is also observed in the present study for "as received"

Figure 7.15a

Unetched 150° indentation made under 9.8 N load on soda-lime-silica at 573°K.

Scale: 1mm=0.8μm

Figure 7.15b

As above but etched 20 seconds.

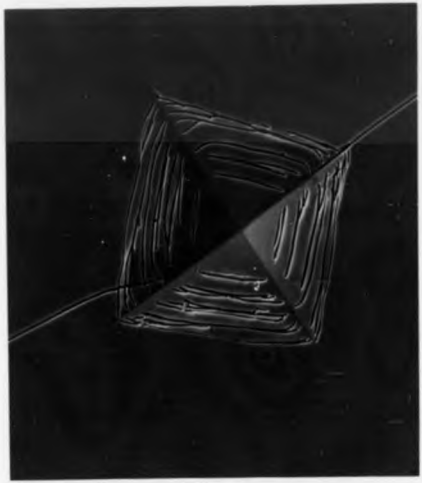

FIGURE 7.16 Present measurements of Vickers Hardness of Soda-lime-silica compared to some previous results

FIGURE 7.17 Hardness measurements for Soda-lime-silica made with various included angle. (Typical errors at different loads indicated by error bars).

surfaces. However, at higher loads the present results are in agreement with those of Stavrinidis (1980).

The present results for the different indenters over the loading range 0.29 to 49 N are compared in Figure 7.17 .

7.6 Fused Silica.

Figure 7.18 shows a Vickers indentation on a plane surface of fused silica at a load of 19.6 N. The apex of the indentation is seen surrounded by a central ring. Beyond this ring covering the remainder of the indent contact area, are numerous features, mostly running parallel to the facet strike. The traces of four cracks can be seen radiating from each of the indentation corners. To the upper right hand corner a large segment has fallen away to expose a conical surface dipping into the specimen from the boundary of the central ring outwards. On this surface and parallel to the to the dip direction are the traces of cracks that radiate from the centre of the indentation.

All the above features can be identified with those recognised by previous authors for Vickers indentations on fused silica. The central ring corresponds to the first ring crack initiated at the edge of the contact area as the indenter penetrated. The exposed conical surface therefore corresponds to the surface of the initial cone crack developed from this ring crack. The numerous traces of further ring cracks, initiated as the contact area expanded are seen on the facet sufaces, although not all of these

Figure 7.18

Vickers 136° indentation made under 19.6 N load on fused silica.

Scale: 1mm=1.4μm

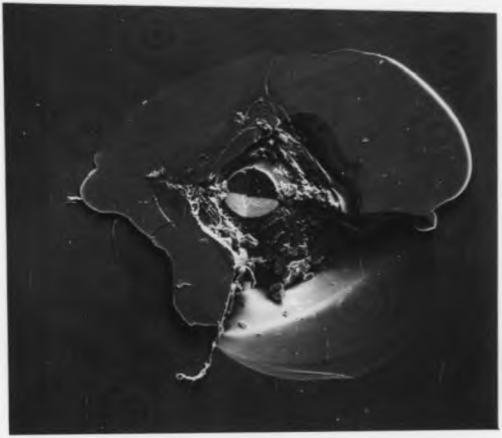

would necessarily have developed to the same extent as the exposed cone crack. The cracks at the indentation corners are the traces on the indentation surface of median cracks. The irregular shaped cracks surrounding the indentation and apparently causing large areas of the surface to break away, are probably the outermost cone cracks that have developed laterally upon unloading.

Figure 7.19 illustrates cone crack traces on the surface of a 150° indentation made under a load of 2.94 N. Cracks can often be traced crossing over to neighbouring facets without disruption at the pyramidal edges, especially near the indentation centre where it is possible to trace near-complete rings. However, away from the centre, cracks traversing the pyramidal edges show some form of consistent subsidiary cracking as the cracks turn sharply. Whereas flow lines on the surface of soda glass indentations tend to be straight and parallel to the strike of the facets, cone crack traces are clearly curved. The shadows accompanying cone cracks, always towards the centre of the indentation, help to indicate that the cracks dip away from the apex into the bulk.

Figure 7.20 is a half surface and section view of a 125° indentation at a load of 2.94 N. On the sectioned plane three types of crack can be distinguished by their orientation. Firstly, a single, vertical crack is found beneath the apex of the indentation. Secondly, to either side of the indentation, runs a large crack inclined at approximately 40° to the indentation surface. Two cracks almost parallel to the surface are seen below the

Figure 7.19

150° indentation made under 2.94 N load on fused silica.

Scale: 1mm=0.71μm

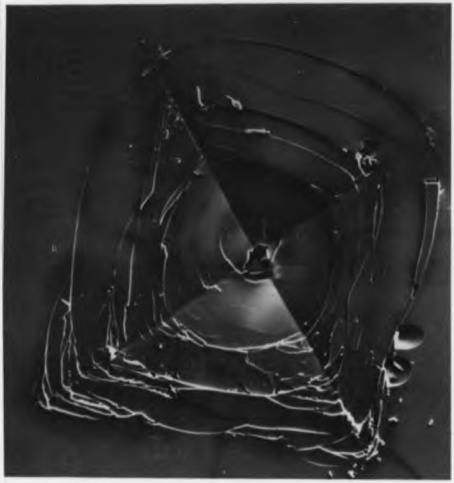

Figure 7.20

Half surface and section view of a 125° indentation on fused silica made under a load of 2.94 N .

Scale 1mm=0.8μm

impression and either side of the vertical crack. The appearance of these cracks has been enhanced because segments have broken off the sectioning plane to expose the crack edges, now obvious as they charge in the electron beam. Two whole facets remain on the indent surface and within the contact area of the impression at least two cracks are seen, clearly open in places and from this viewing angle, approximately circular. A relatively large amount of debris has remained on the indentation despite slight etching.

The three crack types on the sectioned plane correspond to those previously found with sectioned Vickers indentations on fused silica as described in Chapter Five. The vertical crack beneath the apex is the median crack and the two cracks almost orthogonal to this are the lateral cracks. The inclined cracks to either side of the indentation are the dominant cone cracks and it is the traces of these that appear on the facets as ring cracks. Unfortunately the deformed zone beneath the indentation is not well illustrated by this example but no visible flow lines appear to be present.

7.7 Problems with Sectioned Indentations

In evaluating the information obtained from so-called sectioned indentations it should be remembered that these do not provide a true post-indentation cross-section of a normal indent and it may be wise to think of these as "virtual" sections. As described in Chapter Six, the effect of indenting well behind the tip of a crack is to indent

across two abutting edges of glass, and the opposing "sections" show little resemblance to each other; indentations ahead of a crack either shattered as the sectioning crack was extended or were not intersected by the crack. Indenting on healed portions, or at the very tip of an open crack, proved most successful in producing "clean", if virtual, and non-matching, sections of indents.

Occasionally, some features definitely match on opposite sections. This not only includes fractures but also some individual flow lines which would appear to indicate that whatever initiated the flow surface on one half of the sectioned indentation is also present in the glass network in the imediate region of the opposite half.

Other ambiguities can arise and this is well illustrated by the sections of an indentation on a sample of silica illustrated in Figures 7.21a to 7.22 and schematically in Figure 7.23. Figures 7.21a and 7.21b are the adjacent sections. Both figures illustrate the shattered nature of such indentations: the indentation profile is not apparent and there is a wealth of debris. A series of fine, curving lines, labelled AA', BB' etc. appear on each section and the line spacing provides evidence to match the two sections. Figure 7.22 illustrates one section after 20 seconds etching: most of the debris has now been removed together with further segments of the material immediately beneath the former apex, and although the curved lines AA', BB' are still visible, their structure appears to have been changed.

After the first optical examination, these lines were

Figure 7.21a

Deformation beneath a 125° indentation made under a load of 49 N on fused silica. Section A.

Scale: 1mm≈0.8μm

Figure 7.21b

As above but opposing Section B

Figure 7.22

Same as Figure 7.21b but etched for 20 seconds.

Scale: 1mm=0.8μm

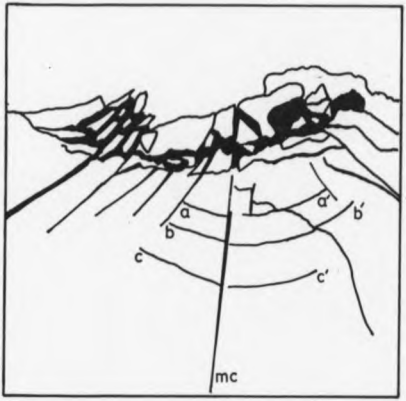

FIGURE 7.23 Schematic representation of the 125° indentation on fused silica (FIGURES 7.21a to 7.22) that illustrated curved basal cracks.

aa' }
bb' } curved basal cracks
cc' }

mc = median crack

thought to be flow lines similar to those found in soda glass. However, later scanning electron microscopy provided persuasive evidence that they are in fact associated with steps in the sectioned surface produced, presumably by elastic relaxations, where small lateral cracks emerge. The white bands associated with each of the curved lines in the electron micrograph of Figure 7.21a are believed to be due to penetration of the beam through the edges of the steps which then allows an additional signal, due to the emission of electrons from the rear of the step, to be detected, Watt (1986).

The electron micrograph in Figure 7.21a shows a well-developed, open median crack which is matched by a rather fine line on the other section, Figure 7.21b . The matching trace can be followed, despite the obscuring debris, at least down to the point marked P. After etching, it is clear that the lower portion of trace on this section corresponds not to a crack, but to a trail of fine etch pits, Figure 7.22. Other collections of pits can be seen along the curved lateral cracks especially in areas where debris collection was heaviest.

It is suggested that whilst this indent was being produced, fine debris particles from the shattered areas under the indenter fell into the gap between the opposing virtual sections, to lodge near the steps formed by the emerging cracks, compare Figures 7.21a and 7.21b . Evidently, as the adjacent surfaces came together again and the specimen relaxed during unloading, the trapped particles caused small abrasions in the surfaces. These,

together with the remaining debris, enhance the visibility of the feint lateral cracks in the optical microscope and are developed into pits on subsequent etching, Figure 7.22 .

Even if this is but part of the explanation of the features on this specimen, the observations underline the need to exercise extreme care in the interpretation of marks found on this kind of virtual section.

CHAPTER EIGHT

DISCUSSION

8.1 Introduction.

A summary of the present results concerning indentations will be followed by a comparison with previous results and a preliminary discussion.

Finally, the consequences of the results obtained in both the indentation and the spontaneous cracking experiments for models of the fracture process in glasses will be considered.

8.2 Summary of Results.

A dominant feature beneath indentations on soda glass is the pattern of intersecting lines. All indentations made by pyramidal indenters with either a 136° or a 125° included angle showed such patterns, but a 150° indenter at very low loads produced small impressions with no sign of this kind of feature.

Progressive etching of an indented surface revealed traces where this line pattern approaches or outcrops at the free indentation surface. The line pattern corresponds to a "virtual" section through a series of three-dimensional, curved surfaces; clearly these surfaces are not cracks: the individual lines meet at angles other than 90°, cross one-another and are kinked at points of intersection.

Virtual sections of indentations on soda glass showed an increase in the line spacing from the apex out towards

the edge of the indent; some lines immediately below the apex are only just resolved by scanning electron microscopy whereas the dominant outer lines could often be seen optically. Indentations made under the greatest loads produced the greatest number of individual lines. The largest kinks (up to 5 microns long) were always found at the intersections of the outer, more prominent lines. These outer lines were more rapidly attacked during etching than those immediately beneath the indentation apex.

The general distribution of the cracks which usually accompany indentation was similar for all three indenters. For loads of 1 N and greater, cracks extended from each of the four corners on the indentation surface and when viewed in section these could be seen to correspond to median cracks.

The saucer-shaped, lateral fractures, known to occur during unloading, cause extensive flaring in the image when an indent is viewed in plan with incident light. The sectioned indentations in soda glass showed clearly the shape and disposition of these cracks.

For fused silica, the appearance of the regions surrounding indentations is very different from that on soda-lime-silica. Silica indentations commonly shatter at higher loads and this limits the examination of the region beneath indentations. However, no sign of a pattern of intersecting lines like that found with soda glass was ever observed.

The general form of the fractures accompanying indentation of silica was the same for all three indenters.

The indentation surface exhibited a series of irregularly-spaced, concentric "ring" cracks, and cone cracks, dipping steeply into the bulk, extended from some of these. Again, radial cracks appeared at the four indentation corners and could be found as median cracks in section, while large, wing-shaped cracks were found below the apex of the indent. The general form of lateral and median cracking in silica is similar to that in soda glass.

8.3 Comparison With Previous Indentation Results

Previous authors have classified glasses as "normal" or "anomalous" in part according to whether flow lines are associated with Vickers indentations. So-called anomalous glasses such as silica do not exhibit flow lines on the virtual sections of 136° indentations and it is usually argued that the indentations are produced by a process of compaction of the glass network to give a denser material, Arora et al (1979), Hagan and van der Zwaag (1984).

The results described here show that for both soda-lime-silica and fused silica the distinctive forms of behaviour are also to be found with 150° and 125° pyramidal indenters and therefore cannot simply be attributed to the differences between the tensile surface strain imposed by the indenter and that sustainable by the materials.

No new types of feature were found in the course of the present study: for all three indenters, the distributions of lines and cracks are broadly similar to those reported by earlier workers for Vickers indenters. However, some evidence in the virtual section of a 150°

indent in soda-lime-silica suggests that appreciable differences of scale can occur in the line patterns even on a single specimen.

Lawn and Swain (1975) show that the disposition of these lines in normal glasses correspond to the major shear stress trajectories beneath a point load on the surface of an isotropic elastic material. Detailed examination of the line patterns under pyramidal indentations, whether in plan after etching or in virtual section, provides only limited views of what must be a complex, three-dimensional set of intersecting surfaces. Nevertheless, the fact that the lines intersect and kink offers persuasive evidence that these are the traces of surfaces across which shear displacements large compared with interatomic distances have occurred; the traces revealed by etching indentations on uncracked specimens, described in this work, lend confidence to the belief that these features are not just artifacts caused by the sectioning technique.

Further support can be inferred from the consistency of the behaviour of the lines in the patterns: the largest intersection kinks were invariably found on the most prominent lines which occur towards the periphery of the deformed zone, where the greatest displacement of material is required; and these prominent lines show the fastest etching rates which in turn implies they are associated with the greatest structural disturbances, Pampillo (1972), a likely consequence of greater shear displacement across a surface whatever atomic processes are involved.

Hagan and van der Zwaag (1984) claimed to be able to recognise two separate types of line in the virtual sections of indentations on normal glasses: "concentric" lines centred about the apex of the indentation and "spiral" lines that approach the indentation surface at one extremity (Figure 8.1). No such subdivision of flow lines was evident on any of the specimens examined in the course of the present study. Incidentally, Hagan and van der Zwaag also claimed to recognise inhomogenous densification in silica glass in the form of densification contours. In the present study, the only features found with a corresponding configuration were the curved cracks illustrated in Figures 7.21a to 7.22 . The nature of these features is not too clear under optical microscopes and it may be that examples of such fractures were misinterpreted by the previous authors.

Ernsberger (1968) and Peter (1970) have suggested that at least limited densification contributes to indent formation in soda-lime-silica, citing as evidence a zone beneath the indentation which appears to exhibit a higher refractive index. Hagan and van der Zwaag (1984) have presented sections of 150° conical indentations that show "flow line free cores" similar to those found in our experiments for 150° pyramidal indenters.

Our discovery of fine-scale flow lines between some major lines serves to emphasise the difficulty in determining whether the deformation is always localised, with traces of the shear surfaces visible, or whether there is a contribution from a quasi-homogeneous shearing of the

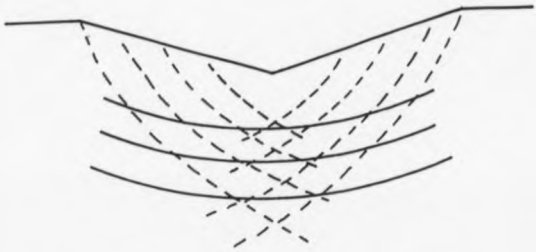

FIGURE 8.1 Classification of flow lines in soda lime silica after Hagan and van der Zwaag (1984).

Solid lines = concentric flow lines
Broken lines = intersecting spiral flow lines

network and (or) some compaction of the network structure. The critical evidence required to separate these possibilities is unlikely to be found using the present virtual sectioning techniques and pyramidal indenters.

Despite some ambiguities in the overall picture, the occurrence of individual, well-spaced surfaces on which major displacements occur implies at least partial inhomogeniety in the response of the glass to the indentation stress field and raises the obvious question concerning what determines the positions of individual large-scale flow surfaces.

While it may be that, as for crystalline materials, the displacement does not take place simultaneously over the whole of the shear surface but in a progressive manner, and a Volterra, elastic dislocation would mark the moving boundary of the displaced material on that surface, there will be no preferred slip planes and the atomic configuration of the "dislocation" would probably not be regular or even the same from one position to another.

It has been suggested that the intersection kinks in flow line patterns act as the origins of the median and secondary radial cracks, Hagan (1980). In principle, one would expect some form of gap to be generated by the intersection of shear surfaces whatever the mechanism responsible, but it is hardly necessary to go as far as Hagan and compare flow line intersection in glasses with void formation in crystals by the pile up of dislocations. Although the idea of kinks nucleating cracks is attractive, there is little direct evidence: certainly many cracks

transect kinks, but it is not clear that the kink served as the origin; on a given virtual section, not all cracks transect a kink and not all kinks have a crack through them. Whatever their origins, the very different final size and configuration of the median and secondary radial cracks in soda glass must be determined by the stress distribution beneath the indenter.

Comparing the fractures in soda glass with fused silica is interesting in this respect. In silica, although part of the median cracks still lie within the deformed zone, there are no small radial cracks and, obviously, no kinks since there are no detectable flow lines. Presumably, the extremely high tensile stresses beneath the indenter are adequate to rupture the network and then drive a crack. It is worth noting that there would need to be at least three independent sites of median crack initiation to produce the radial cracks at all four corners which are usually visible on the indentation surface, since two cracks can not cross one another.

The ring and cone cracks formed in silica glass have been attributed to tensile stress at the contact boundary between glass and indenter. Although not regularly reported, such ring fractures are occasionally produced in soda glass, for example around the periphery of the indentation in Figure 7.14a . Perhaps the lower frequency of these fractures on soda-lime glass is due to the slightly lower stresses around the indenter (reflected in a lower diamond pyramid hardness) and the superior surface condition of commercial soda-lime-silica glass which

offers fewer surface flaws to initiate ring cracks. The surface ring cracks in soda glass very rarely, if ever, develop into cone cracks of the form common in silica. It may be that this is because the downward growth of the cones is frustrated by subsurface radial cracks as appears to have occurred in the specimen shown in Figure 7.3 .

8.4 Models of Glass Fracture

A fundamental question concerning the mechanical behaviour of glass of some interest, at least in the laboratory where the present experiments were carried out, is "what role does flow play in the fracture of glass ?", Gunasekera (1970), Weidmann (1973), Stavrinidis (1980) and Holloway (1983). The two series of experiments described here have a direct bearing on this question and we should consider whether the results offer any new insights.

The spontaneous extension of cracks was of potential interest since it was thought the process may have given some information concerning crack tip processes and environment-sensitive fracture. However, if our interpretation of the present results is correct and "spontaneous cracking" is simply the extension of pre-existing microcracks by locally developed mechanical stresses, then the effect poses new problems rather than shedding light on the fracture of glass.

The differences in the indentation behaviour of normal and anomalous glasses are not reflected in their tensile fracture behaviour. That plastic flow of some form occurs under an indenter has long been recognised but no sign of

inelastic, permanent deformation has been detected accompanying fracture. However, the argument that plasticity also occurs during fracture on a scale that may not leave visible evidence has received support, in part to explain why the fracture energy exceeds the surface free energy of glass.

Essentially two schools of thought have developed to describe the nature of the crack tip. On the one hand fracture is envisaged as the sequential ruture of atomic bonds at an atomically sharp tip, Lawn (1983). The process may be influenced by the environment, notably the attack of strained bonds at the crack tip by aqueous solutions, Michalske and Freiman (1983), Michalske and Bunker (1987). On the other hand, the tip is considered to be rounded by some form of inelastic deformation in a zone ahead of the open crack; it is in this zone that extra energy is dissipated in the course of extending the crack, Hillig (1968), Weidmann (1973), and Weidmann and Holloway (1974a,b,c).

The results of the work described here offer little to support one or the other of these hypotheses. In the case of spontaneous cracking, it is evident from the results for slow crack propagation under applied loads (Figures 3.14 and 3.15), that the alkaline solutions used do not directly aid bond rupture. However, what they can clearly provide, in the absence of an applied stress, is an additional source for the crack driving stress, as the result of some chemo-mechanical reaction. Therefore, no significance is made of the fact that soda glass does not

exhibit spontaneous cracking; it is simply that suitable chemical reactions do not occur with this composition.

The use of pristine tensile strength to predict the permanence of indents or the form of deformation that accompanies them is clearly incorrect. Indenters imparting very low surface tensile strains persist in producing permanent impressions despite the fact that such strains can be accommodated elastically. In addition, the form of deformation appears the same despite differences in surface strain. It would seem likely that the onset of the shear flow found in normal glasses depends upon a complex criterion, involving the three dimensional stress state.

The macroscopic strength of normal artifacts of glass is governed by the presence of surface flaws and discontinuities which act as the origin of failures. Some form of shear or slip has been demonstrated on localised surfaces in normal glasses under an indenter and even though we can not specify the critical stress conditions required, there would appear to be no obvious reason why such flow should not occur in tension. So that, from a logical point of view we could ask: if flow does not occur at least locally in normal glasses during fracture, why not?

If intersecting slip does initiate cracks, this may explain why pristine strengths often coincide with the tensile yield stress calculated from hardness numbers after allowing for the unusually high strain, Marsh (1964a). This might also account for the discrepancy between observed pristine strengths and theoretical values based on models

of perfectly brittle behaviour. However, the argument is not straightforward: anomalous glasses such as silica also exhibit similar correlation between pristine strength and hardness despite their different indentation behaviour.

8.5 Conclusion

The spontaneous fractures reported in this thesis appear to be stress driven and, if this is so, can shed no light on the nature of the crack tip or the fracture process in glass. However, that is not to say that the existence of such a process is not without practical significance and academic interest.

The indentation tests have shown that the criterion for permanent deformation beneath an indenter is certainly not simply the magnitude of tensile surface strain imposed. The patterns of cracks and lines previously found beneath Vickers indentations on soda and silica glass have been confirmed and their presence established for both 125° and 150° pyramidal indenters. Some new detail has been observed; of particular interest is the discovery of very fine scale flow lines in soda glass as this raises the possibility that more homogeneous shearing may occur than had been previously envisaged. However, our observations do not preclude the possibility that densification contributes to the formation of an indent in both normal and anomalous glasses.

The possible ambiguities of virtual sectioning to explore indentation structure can now be avoided by etching normal, unsectioned indentations. Signs of the subsurface

localised shear deformation can still be recognised using this method.

APPENDIX

Angular Transducer: Operation and Calibration.

A d.c./d.c. angular position sensor (Penny and Giles Ltd.) was used in conjunction with the double torsion machine to aid the measurement of crack length in specimens tested under applied load. The angular transducer was connected to the shaft of the main loading arm and so directly measured the rotation of this arm. The input voltage for the transducer was from a stabilised power supply (Coutant Ltd.) and the variable output was read with a digital multimeter (Schlumberger Ltd.) or continuously recorded using a flat-bed pen recorder (J.J. Instruments Ltd.).

The transducer was calibrated using the equations derived by Timoshenko and Goodier (1970) to decribe the elastic response of double torsion specimens under four point bending. From this theory it can be shown that:

$$G = 3f^2m^2 / \mu b^4 w(1-0.63b/w) \qquad [A1]$$

and also,

$$G = \mu\theta b^2 w(1-0.63b/w) / 12L^2 \qquad [A2]$$

where μ is the elastic shear modulus, f the force at each of the four loading points, m the distance between the loading points on one arm of the specimen, b the specimen thickness, w its width, θ the angular deflection of the one half of the specimen under torsion (in radians) and L is the crack length. (see Figure A.1).

Eliminating G between equations A1 and A2 gives equation A3 which provides a relationship between θ and L:

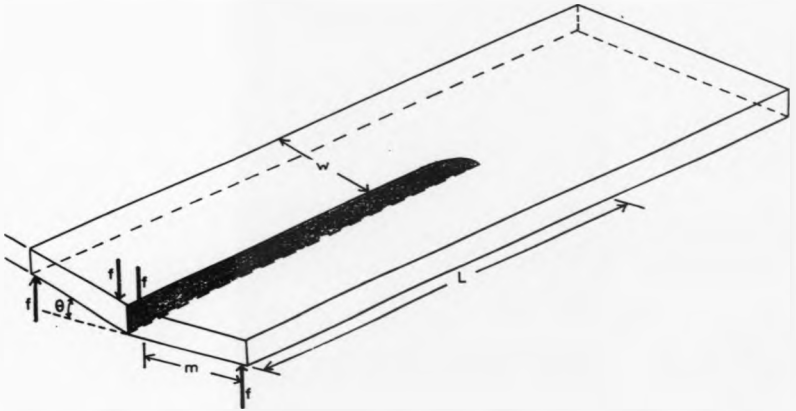

FIGURE A.1 Simplified representation of the loading configuration during the production of macroscopic cracked specimens using a double torsion machine.

$$\theta = [\ 36L^2f^2m^2\ /\ \mu^2b^6w^2(1-0.63b/w)^2\ ]^{1/2} \qquad [A3]$$

and by substituting for $fm = FR$, where F is the force acting on the pulley wheel of the torsion machine with a radius R we finally obtain the relationship used for the calibration between angular deflection of the loading arm and the crack length:

$$\theta = [\ 36L^2(FR)^2\ /\ \mu^2b^6w^2(1-0.63b/w)^2\ ]^{1/2} \qquad [A4]$$

Specimens of different thickness, width and under various loads (hence propagating cracks over a range of velocities) were used during calibration. Using a cathometer, the exact lengths of cracks were measured regularly together with the corresponding output voltage, V, from the angular transducer. Then for these crack lengths the angular deflection was calculated using equation A4 and plotted against voltage.

A straight line relationship was found between θ and V and a calibration factor equal to $0.02095 \pm 2.9*10^{-3}$ radians per volt was obtained from the slope of this line.

Hence, during subsequent testing a voltage change ΔV was converted to an angular deflection $\Delta\theta$ and so to a crack propagation ΔL. Together with a measurement of time the crack velocity could be calculated.

Crack velocity measurements made by this method were subject to a total error of 20.2% of which an unavoidably large contribution was provided by the standard deviation in the calibration of θ/V, viz 13.8%. The remaining error was due to operational errors in the measurement of the specimen thickness and width and the radius of the torsion machine pulley.

REFERENCES

Adams, P.B. (1974) Proc. 10th Int. Glass Cong., Kyoto, July 1974.

Ainsworth, L. (1954) J. Soc. Glass Technol. 38 479T

Anderson, O.L. and Diennes, G.J. (1960) "Non-Crystalline Solids".Ed. V.D. Frechette, Wiley, New York P.449.

Arora, A., Marshall, D.B., Lawn, B.R. and Swain, M.V. (1979) J. Non-Cryst. Solids 31 415

Brueche, E. and Poppa, H. (1956) J. Soc. Glass Technol. 40 513T

Budd, S.M. (1961) phys. Chem. Glasses 2 111

Charles, R.J. (1958) J. Appl. Phys. 11 1549

Cohen, H.M. and Roy, R. (1961) J. Am. Ceram. Soc. 44 523

Dick, E. (1970) Glastech. Ber. 43 16

Doremus, R.H. (1973) "Glass Science". Wiley and Sons, New York.

Doremus, R.H. (1979) "Treatise on Materials Science and Technology", Vol. 17, Glass II, (M.Tomozawa and R.H.Doremus, eds.), Academic Press, New York.

Douglas, R.W. and Isard, J.O. (1949) J. Soc. Glass Technol. 33 289

Ernsberger, F.M. (1968) J. Am. Ceram. Soc. 51 545

Ernsberger, F.M. (1980) Phys. Chem. Glasses 21 146

Fine, G.J. and Danielson, P.S. (1988) Phys. Chem. Glasses 29 134

Finkel, V.M. and Kutnik, I.A. (1962a) Soviet. Phys. Dokl. 7 231

Finkel, V.M. and Kutnik, I.A. (1962b) Soviet Phys. Solid St. 4 1038

Frieman, S.W. (1985) "Strength of Inorganic Glass", NATO Conf. Series VI, Mat. Sci. vol.11, Proc. of NATO advanced research workshop entitled Strength of Glass, March 1983, Algarve, Portugal, Plenum Press (New York) 1985.

Goodman, C.H.L. (1986) Phys. Chem. Glasses 27 27

Goodman, C.H.L. (1987) Glass Technol. 28 19

Griffith, A.A. (1920) Phil. Trans. R. Soc. A221 163

Gunasekera, S.P. (1970) MSc. Thesis, University of Keele

Hagan, J.T. (1979a) J. Mat. Sci. 14 462

Hagan, J.T. (1979b) J. Mat. Sci. 14 2975

Hagan, J.T. (1980) J. Mat. Sci. 15 1417

Hagan, J.T. and Swain, M.V. (1978) J. Phys D: Appl. Phys. 11 2091

Hagan, J.T. and van der Zwaag, S. (1984) J. Non-Cryst. Solids 64 249

Hench, L.L. and Clark, D.E. (1978) J. Non-Cryst. Solids 28 83

Hillig, W.B. (1968) "Microplasticity", Ed. C.J. M. Mahon, jr., Wiley and Sons, New York, P.383.

Holland, L. (1964) "The Properties Of Glass Surfaces", Chapman and Hall, London.

Holloway, D.G. (1983) "A Look at the History of Glass Strength" in "Strength of Inorganic Glasses", NATO Conf. Series VI, Mat. Sci. vol.11, Proc. of NATO advanced research workshop entitled Strength of Glass, March 1983, Algarve, Portugal, Plenum Press (New York) 1985.

Hudson, G.A. and Bacon, F.R. (1958) Am. Ceram. Soc. Bull. 37 185

Johnson, J.W. and Holloway, D.G. (1966) Philos. Mag. 14 731

Johnson, J.W. and Holloway, D.G. (1968) 17 899

Kies, J.A. and Clark, A.B.J. (1969) Proc. 2nd Int. Conf. on Fracture, Brighton 1969, Chapman and Hall, London, 1970.

Lavoisier, A.L. (1770) Mem. Acad. Sci., Paris 73 125

Lawn, B.R. (1983) J. Am. Ceram. Soc. 66 83

Lawn, B.R. and Fuller, E.R. (1975) J. Mat. Sci. 10 2016

Lawn, B.R. and Swain, M.V. (1975) J. Mat. Sci. 10 113

Lawn, B.R. and Wilshaw, R (1975) J. Mat. Sci. 10 1049

Mallinder, F.P. and Proctor, B.A. (1964) Phys. Chem. Glasses 5 91

Marsh, D.M. (1964a) Proc. Roy. Soc. A 279 420

Marsh, D.M. (1964b) Proc. Roy. Soc. A 282 33

Metcalfe, A.G., Gulden, M.E. and Schmitz, G.K. (1971) Glass Technol. 12 15

Michalske, T.A. and Bunker, B.C. (1987) J. Am. Ceram. Soc. 70 780

Michalkse, T.A. and Frieman, S.W. (1983) J. Am. Ceram. Soc. 66 284

Michalske, T.A. and Fuller,jr. E.R. (1985) J. Am. Ceram. Soc. 68 586

Neely, J.E. and Mackenzie, J.D. (1968) J. Mat. Sci. 3 603

Newton, R.G., Holloway, D.G. and Hench, L.L. (1979) Ann. 8th Cong. Assoc. Int. du Verre, London and Liverpool, 1979, Liege.

Nordberg, M.E., Mochel, E.L., Garfinfel, H. and Olcott,J.S. (1964) J. Am. Ceram. Soc. 47 215

Oka, Y., Ricker, K.S. and Tomozawa, M. (1979) J. Am. Ceram. Soc. 62 631

Outwater, J.O. and Gerry, D.J. (1967) Mod. Plast. 45 156

Pantano,jr. C.G., Dove, D.B. and Onoda,jr. G.Y. (1976) J. Vac. Sci. Technol. 13 414

Paul, A. (1977) J. Mat. Sci. 12 2246

Peter, K.W. (1970) J. Non Cryst. Solids 5 103

Prod'homme, M (1968) Phys. Chem. Glass. 9 101

Randal, J.T., Rooksby, H.P. and Cooper, B.S. (1931) J. Soc. Glass Technol. 15 54

Roberts, G.J. and Roberts, J.P. (1964) Phys. Chem. Glasses 5 26

Rooke, D.P. and Cartwright, D.J. (1976) "Stress Intensity Factors", H.M.S.O.

Sakaguchi, S., Sakawi, Y., Abe, Y. and Kawasaki, T. (1982) J. Mat. Sci. 17 2878

Samuels, L.E. and Mulhearn, T.O. (1957) J. Mech. Phys. Solids 5 125

Schonert, K., Umhauer, H. and Klemm, W. (1969) Proc. 2nd Int. Conf on Fracture, Brighton 1969, Chapman and Hall, London, 1970.

Shand, E.B. (1958) "Glass Engineering Handbook", Mc Graw Hill, New York.

Stavrinidis, B. (1980) PhD. Thesis, University of Keele

Stavrinidis, B. and Holloway, D.G. (1983) Phys. Chem. Glasses 24 19

Tabor, D. (1951) "The Hardness Of Metals", Clarendon, Oxford.

Taylor, E.W. (1949a) Nature 163 323

Taylor, E.W. (1949b) Nature 163 1150

Taylor, E.W. (1950) J. Soc. Glass Technol. 34 69T

Timmoshenko, S.P. and Goodier, J.N. (1970) "Theory Of Elasticity" 3rd Ed. McGraw Hill, New York.

Tomozawa, M., Oka, Y. and Wahl, J.M. (1981) J. Am. Ceram. Soc. 64 C-32

Warren, B.E. (1937) J. Appl. Phys. 8 645

Watt, I. (1986) Optical and Electron Microscopy 19 6

Weidmann, G.W. (1973) PhD. Thesis, University of Keele

Weidmann, G.W. and Holloway (1974a) Phys. Chem. Glasses 15 68

Weidmann, G.W. and Holloway, D.G. (1974b) Phys. Chem. Glasses 15 116

Weidmann, G.W. and Holloway, D.G. (1974c) "Symposium On Strength Of Glass And Glassware", Soc. Glass Technol. 1974. (Extended Abstracts).

Wiederhorn, S.M. (1967) J. Am. Ceram. Soc. 50 407

Zachariasen, W.H. (1932) J. Am. Chem. Soc. 54 3841